Hitting time of rapid intensification onset in hurricane-like vortices

Cite as: Phys. Fluids **33**, 096603 (2021); https://doi.org/10.1063/5.0062119
Submitted: 02 July 2021 • Accepted: 20 August 2021 • Published Online: 14 September 2021

Wai-Tong (Louis) Fan, Chanh Kieu, Dimitrios Sakellariou, et al.

Physics of Fluids ARTICLE scitation.org/journal/phf

Hitting time of rapid intensification onset in hurricane-like vortices

Cite as: Phys. Fluids 33, 096603 (2021); doi: 10.1063/5.0062119
Submitted: 2 July 2021 · Accepted: 20 August 2021 ·
Published Online: 14 September 2021

Wai-Tong (Louis) Fan,[1,a)] Chanh Kieu,[2,b)] Dimitrios Sakellariou,[1] and Mahashweta Patra[2]

AFFILIATIONS

[1]Department of Mathematics, Indiana University Bloomington, Bloomington, Indiana 47405, USA
[2]Department of Earth and Atmospheric Sciences, Indiana University Bloomington, Bloomington, Indiana 47405, USA

[a)]Electronic mail: waifan@iu.edu
[b)]Author to whom correspondence should be addressed: ckieu@indiana.edu

ABSTRACT

Predicting tropical cyclone (TC), rapid intensification (RI) is an important yet challenging task in current weather forecast due to our incomplete understanding of TC nonlinear processes. This study examines the variability of RI onset, including the probability of RI occurrence and the timing of RI onset, using a low-order stochastic model for TC development. Defining RI onset as the first hitting time for a given subset in the TC-scale state space, we quantify the probability of the occurrence of RI onset and the distribution of the timing of RI onset for a range of initial conditions and model parameters. Based on asymptotic analysis for stochastic differential equations, our results show that RI onset occurs later, along with a larger variance of RI onset timing, for weaker vortex initial condition and stronger noise amplitude. In the small noise limit, RI onset probability approaches one and the RI onset timing has less uncertainty (i.e., a smaller variance), consistent with observation of TC development under idealized environment. Our theoretical results are also verified against Monte Carlo simulations and compared with explicit results for a general one-dimensional system, thus providing new insights into the variability of RI onset and helping better quantify the uncertainties of RI variability for practical applications.

I. INTRODUCTION

Rapid intensification (RI) is an inherent feature of hurricanes (also known as tropical cyclone or TC) by which a TC intensifies quickly in a very short period of time.[1] Predicting RI onset is therefore of great importance in operational TC forecast such that proper and timely risk management and preparation can be initiated.[2–5]

While RI is guaranteed to occur under idealized environment, the probability or the exact moment that RI onset takes place in real-time forecast highly fluctuates as a result of varying environmental conditions.[6,7] Despite progress in improving TC intensity forecast skill, RI prediction has been challenging to date. As shown in, for example, Refs. 8–12, current operational models still have a high false alarm rate and a moderate probability of detection for RI prediction, even at a short 24–36 h lead time. The RI forecast skill is significantly deteriorated as the forecast lead time is extended longer, making it hard to reliably predict RI in real-time applications. With various uncertainties in TC intensity fluctuation related to vortex initial conditions, model errors, boundary conditions, and potential existence of TC intensity chaotic dynamics and random variability,[6,7,13,14] it is necessary to examine to what extent RI onset can be best predicted for future operational applications and model improvement.

From the practical perspective, TC development always contains an intrinsically random process that can never be fully controlled due to the stochastic nature of the atmosphere. Naturally, one then expects RI onset to be impacted by such random variability from the atmosphere, especially during the early stage of TC development that possesses high uncertainties in both the structure and strength. Figure 1 shows an example of TC intensity evolution obtained from the Coupled Ocean Atmospheric Prediction System (COAMPS-TC) model,[15,16] using an ensemble of simulations with small random noises centered on a given initial condition.[17] One notices that the RI onset timing in this ensemble, defined to be the first moment in the model simulation that the maximum surface wind (Vmax) increases by 14.5 m s^{-1} (30 kt) per 24 h, is not a deterministic variable but varies significantly, regardless of how perfect environmental conditions are.

The above random variation of RI onset timing as illustrated by the COAMPS-TC model is in fact just one among many other possible

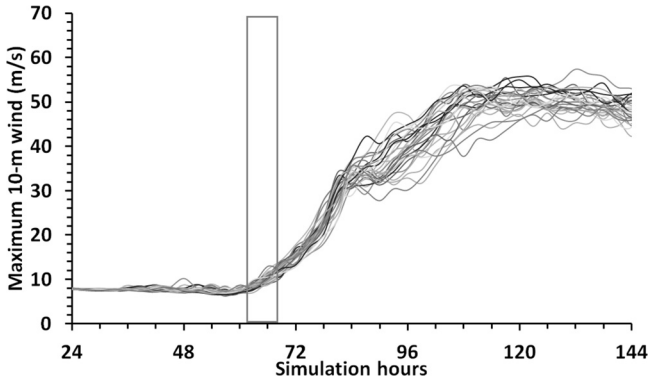

FIG. 1. Time series of the maximum 10 m wind (VMAX) ensemble during the course of idealized simulations using the COAMPS-TC model, under a perfect model scenario. The ensemble is perturbed by small random perturbations at the initial condition as presented in Ref. 17. The gray box denotes the interval at which RI onset time varies among different ensemble members. Here, the RI onset moment is defined as the time into simulation that the VMAX change in the next 24 h is $\geq 14.5\ \mathrm{ms}^{-1}$.

sources of uncertainties related to, for example, boundary and surface layer parameterization, model physics, vortex initial conditions and locations, or potential existence of TC chaotic dynamics.[14,18–21] The combination of all these uncertainties apparently suggests that RI onset should not be treated as a deterministic but more as a stochastic process. How to quantify the probability of RI onset as well as its timing is, nevertheless, an open question in the current TC research.

In this paper, based on the asymptotic hitting analysis for stochastic differential equations (SDE), we study the probability of RI onset as well as the variability of RI onset timing. Our objective is to examine RI onset under idealized conditions such that intrinsic random characteristics of RI onset in the absence of all environmental asymmetries can be investigated. For this purpose, the *first-hitting time* (also known as the *first passage time*) technique for stochastic processes appears to be appropriate and beneficial due to its connection with stochastic analysis. Defined as the moment when a stochastic process first visits a given subset in the state space, the first-hitting time can be directly linked to RI onset time from which the first-hitting time techniques can be applied to study the variability of RI onset as expected. To the best of our knowledge, this approach and its applications to TC development have not been previously explored. As such, we wish to present in this study a theoretical framework that could allow one to rigorously quantify the probability of RI onset as well as the variability of RI onset timing as a function of the ambient environment and TC initial conditions.

The rest of this study is organized as follows. In Sec. II, a stochastic model for TC development is presented, followed by a formal definition of RI onset within the first-hitting time framework. Section III presents theoretical results for the probability of RI occurrence and the distribution of RI onset time. Monte Carlo simulations to verify our theoretical results will be provided in Sec. IV, along with additional insights on the dependence of RI onset on model parameters. Concluding remarks are given in the final section.

II. FORMULATION

A. Stochastic model for TC intensification

With an axisymmetric assumption for TC development, Kieu and Wang[22] presented a simple low-order model that is based on a few fundamental scales of TCs. Unlike common TC balance models, this TC-scale dynamics, which is a modified version of a TC model originally proposed by Kieu[23] and is hereinafter referred to as the modified scale dynamics (MSD) model, is time-dependent and explicitly contains the maximum potential intensity limit as one of its critical points. In the non-dimensional form, the MSD system in Ref. 22 can be summarized as follows:

$$\begin{cases} \dfrac{du}{dt} = pv^2 - (p+1)b - u|v|, \\ \dfrac{dv}{dt} = -uv - v|v|, \\ \dfrac{db}{dt} = bu + su + |v| - rb, \end{cases} \tag{1}$$

where (u, v, b) denote non-dimensional variables that represent the maximum radial wind, the maximum tangential wind, and the warm core anomaly in the TC inner-core region. The parameter p is proportional to the squared ratio of the depth of the troposphere over the depth of the boundary layer, s is an effective tropospheric static stability parameter, and r represents the Newtonian cooling. Detailed derivation of this TC-scale system under the assumption of wind induced surface heat exchange (WISHE) feedback can be found in Ref. 22.

Because of the dependence of frictional forcing and the WISHE feedback on the wind amplitude, the terms containing the absolute sign in Eq. (1), that is, $|v|$, result in two possibilities for TC development corresponding to cyclonic and anticyclonic flows. To ease our subsequent analyses, we will focus only on the regime in the state space where $v > 0$, which corresponds to cyclonic TCs in the Northern Hemisphere. This cyclonic system will be hereinafter explicitly referred to as an MSD_+ system [see Eqs. (69)–(71) in Ref. 22], which is described by the following equations:

$$\begin{cases} \dfrac{du}{dt} = pv^2 - (p+1)b - uv, \\ \dfrac{dv}{dt} = -uv - v^2, \\ \dfrac{db}{dt} = bu + su + v - rb. \end{cases} \tag{2}$$

To simplify our notation, we write this MSD_+ system in the form

$$\frac{d\mathbf{x}(t)}{dt} = \boldsymbol{\mu}(\mathbf{x}(t)), \quad t \geq 0, \tag{3}$$

where $\mathbf{x}(t) \equiv [u(t), v(t), b(t)]$, and the vector field $\boldsymbol{\mu} = (\mu_1, \mu_2, \mu_3) : \mathbb{R}^3 \to \mathbb{R}^3$ is the forcing function of (2), that is,

$$\begin{cases} \mu_1(u, v, b) = pv^2 - (p+1)b - uv, \\ \mu_2(u, v, b) = -uv - v^2, \\ \mu_3(u, v, b) = bu + su + v - rb. \end{cases} \tag{4}$$

While the low-order MSD system is admittedly simple as compared to real TCs, the fact that main TC dynamics can be formulated in such a mathematically closed form is noteworthy here. This is

because this MSD system allows one to obtain different insights into the underlying mechanisms of TC development beyond numerical simulations by full-physics models that one cannot fully control.

Given the above deterministic model (2) for TC development, we next extend it to a stochastic system. Following Ref. 7, stochastic forcing is introduced to the MSD system as an additive Wiener process. Specifically, we consider the stochastic process $\mathbf{X}_t := (U_t, V_t, B_t)$ solving the time-homogeneous Itô stochastic differential equation as follows:

$$d\mathbf{X}_t = \mu(\mathbf{X}_t)\, dt + \varepsilon\, d\mathbf{W}_t, \quad t \geq 0, \tag{5}$$

where $\varepsilon > 0$ is a constant (the diffusion coefficient) that parametrizes the magnitude of the fluctuation of the random forcing, and $\mathbf{W}$ is a standard 3-dimensional Wiener processes. Explicitly

$$\begin{cases} dU_t = (pV_t^2 - (p+1)B_t - U_tV_t)\, dt + \varepsilon\, dW_t^{(u)}, \\ dV_t = (-U_tV_t - V_t^2)\, dt + \varepsilon\, dW_t^{(v)}, \\ dB_t = (B_tU_t + sU_t + V_t - rB_t)\, dt + \varepsilon\, dW_t^{(b)}, \end{cases} \tag{6}$$

where $\{W^{(u)}, W^{(v)}, W^{(b)}\}$ are independent Wiener processes. The use of these independent Wiener processes to represent the random forcing for the MSD system significantly simplifies the problem both theoretically and numerically. For example, a numerical solution to Eq. (6) with a sufficiently small discretization time step Δt can be obtained by using the simple Euler–Maruyama scheme in which a Gaussian random variable with variance $(\Delta t)\varepsilon^2$ is added to each state variable in every iteration.[7,24] Figure 2 shows an illustration of numerical simulations of the MSD system (6) for 30 different realizations, using the same method and parameters as in Ref. 7. One notices apparently from this result that the MSD system displays RI for many realizations, while a few realizations quickly decay. For those that display RI, notice also that the RI onset timing varies as well (see the crosses in Fig. 2). How the probability of RI occurrence and its related variability depend on model parameters or vortex initial conditions is the main question we wish to tackle herein.

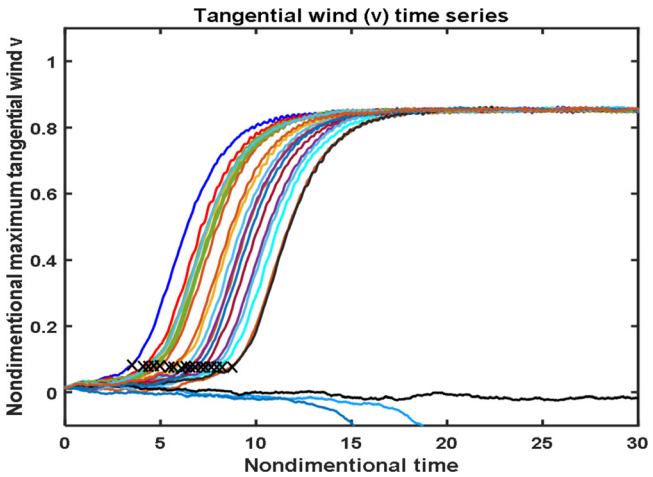

FIG. 2. Time series of the v component of the MSD system (6), which is obtained from a 30-member Monte Carlo simulation, using the same set of parameters (p, r, s) as in Ref. 7 and initial condition of $(u = 0, v = 0.01, b = 0)$. The crosses denote the RI onset moment, which is defined as the first time into the simulation that the v component starts to rapidly amplify, similar to the RI onset defined in Fig. 1.

It should be mentioned that the closed form of the MSD system as given by (6) is important in this study, as one can employ rigorous mathematical tools such as stochastic calculus and asymptotic analysis to study RI onset. One could of course use full-physics models such as the COAMPS-TC to examine the stochastic nature of RI onset as shown in Fig. 1. Note however that the larger computational and storage requirement of the full-physics models generally prevent one from carrying out a large number of simulations to obtain significant statistics, let alone analyzing the various nonlinear contribution of different large-scale factors. In this regard, the Itô SDE (6) is useful for our theoretical analyses herein. The meaning and the well-posedness of these SDEs can be found in standard textbooks such as Ref. 25 and will not be discussed further here.

B. RI onset definition

To assess the occurrence (and failure) of RI onset and to quantify the distribution of RI onset timing, it is necessary to introduce a formal definition of RI onset such that rigorous analyses can be obtained. Given the previous studies on the first-hitting time for stochastic systems, we herein define RI onset time as the first moment that the V component reaches a given level $\ell \in (0, \infty)$; afterward, RI is guaranteed to occur. Analyses of the MSD system showed indeed that such an RI onset level always exist,[23] because the MSD system contains a single stable point at the maximum potential intensity limit (cf. Figs. 1 or 2 and Ref. 7). As such, when V reaches the level ℓ, TC intensification is ensured to rapidly approach the potential intensity state, thus justifying our definition of RI onset here.

Given the above definition of RI onset time, we now investigate the following two specific questions:

(1) **Probability of RI onset occurrence:** whether or not tangential wind (i.e., v) will reach the level ℓ such that RI onset can occur; and
(2) **Variability of RI onset timing:** if RI occurs, what is the statistical distribution of RI onset time?

To be more specific, we introduce the following hitting times for the stochastic MSD system (6):

$$\tau_+ := \inf\{t \geq 0 : V_t = \ell\}, \text{ the first time when } V \text{ reaches } \ell, \tag{7}$$

$$\tau_0 := \inf\{t \geq 0 : V_t = 0\}, \text{ the first time when } V \text{ hits zero (i.e., an initial vortex diesout)}. \tag{8}$$

The *RI onset time* for the SDE (6) is defined to be τ_+. Furthermore, we say that *RI onset occurred* if $\tau_+ < \tau_0$. That is, when the trajectory of v hits ℓ without dying out before that. The condition $\tau_+ < \tau_0$ is needed here, because any tropical disturbance hitting the level $v = 0$ will be considered as being dissipated and so there is no RI for this vortex development in reality.

Due to the stochastic nature of the TC stochastic dynamics, it is apparent that τ_+ is a random variable. As such, our aim is to obtain the probability $\mathbb{P}_{\mathbf{x}_0}(\tau_+ < \tau_0)$ as a function of the initial condition $\mathbf{x}_0 = (u_0, v_0, b_0)$ and the model parameters. Since the initial point can be any point in the state space, we define the function

$$p(\mathbf{x}) := \mathbb{P}_x(\tau_+ < \tau_0), \tag{9}$$

with $\mathbf{x} = (u, v, b)$ a generic point in the state space.

For comparison between the stochastic and deterministic MSD systems, one needs also a deterministic RI onset time T for the ordinary differential equation (ODE) (2), which is defined as follows:

$$T := \inf\{t \geq 0 \,; v(t) = \ell\}. \tag{10}$$

By definition, T the first time the trajectory $[v(t)]_{t\geq 0}$ of (2) hits level ℓ in the absence of all stochastic forcings. It should be noted that one cannot choose a too large value for ℓ, as the MSD system possesses a unique stable point v_*.[22,23] Thus, v will be always attracted to its equilibrium v_* and may never reach ℓ if ℓ is set too large. Hence, it is natural to make the following mild assumption throughout the paper.

Assumption 1. *$0 < \ell < v_*$, where v_* is the v-component of the stable critical point in the phase space (u, v, b) of the ODE (2).*

Under this assumption, T is finite (i.e., the v-component of the ODE must hit level ℓ) if the initial condition $v_0 > 0$. That is, the v-trajectory for the ODE never hits zero so long as the initial value v_0 is positive as proven in Ref. 22.

III. THEORETICAL RESULTS

In this section, we present rigorous analyses of the RI onset probability $p(\mathbf{x}) = \mathbb{P}_{\mathbf{x}}(\tau_+ < \tau_0)$ for the stochastic MSD model (6), along with the conditional probability distribution of τ_+. We recall from our definition (7) of RI onset time that τ_+ is the first time for v to reach level ℓ. Thus, we will apply the asymptotic techniques for SDE to estimate the hitting time in the MSD model (6).

We note first that Eq. (6) has a unique strong solution $\mathbf{X} = (\mathbf{X}_t)_{t\geq 0}$, where $\mathbf{X}_t = (U_t, V_t, B_t)$ is a three-dimensional vector for each time $t \geq 0$. Furthermore, X is a continuous-time strong Markov process with infinitesimal generator $\mathscr{L}$ defined by the following differential operator:

$$\mathscr{L}f(x) = \mu_1 \frac{\partial f}{\partial u} + \mu_2 \frac{\partial f}{\partial v} + \mu_3 \frac{\partial f}{\partial b} + \frac{\varepsilon^2}{2}\left(\frac{\partial^2 f}{\partial u^2} + \frac{\partial^2 f}{\partial v^2} + \frac{\partial^2 f}{\partial b^2}\right), \tag{11}$$

where $\mathbf{x} = (u, v, b)$ is a generic point in the state space of the SDE. Let $p(\mathbf{x}, t)$ be the probability density for $\mathbf{X}_t$; that is, $\mathbb{P}(\mathbf{X}_t \in dx) = p(\mathbf{x}, t)dx$ where $d\mathbf{x}$ is the Lebesgue measure in $\mathbb{R}^3$. Then, $p(\mathbf{x}, t)$ satisfies the Fokker–Planck equation $\frac{\partial p(\mathbf{x},t)}{\partial t} = \mathscr{L}^* p(\mathbf{x}, t)$, where $\mathscr{L}^*$ is the adjoint of $\mathscr{L}$ in the Hilbert space $L^2(d\mathbf{x})$. These facts follow from standard techniques in stochastic calculus as can be seen, for instance, in Ref. 25, Chap. 5.

In principle, (11) enables one to obtain all desired statistics of RI onset time. However, due to nonlinearity of the SDE there is no explicit formula for the density $p(\mathbf{x}, t)$. In Subsections III B and III C, we shall therefore derive formal results for the probability of RI onset and the distribution of τ_+ in the asymptotic limit of small stochastic forcing. These formal connections between SDE and partial differential equation (PDE) are the starting point of more in-depth analysis of the statistics of RI onset time that we can later verify by Monte Carlo simulations.

Remark 1 (Implicit dependence parameters). We note that the process $\mathbf{X} = (U, V, B)$, the generator $\mathscr{L}$, the onset time τ_+, and the extinction time τ_0 all depend on the noise parameter ε and the MSD model parameters (p, r, s). This dependence is important to understand how the probability of RI onset would depend on large-scale environmental factors, but it will be made implicit here to simplify our notation.

A. Probability of RI onset

In the case when the initial value of V is positive (i.e., $V_0 > 0$), it is possible to obtain a simplification for the MSD$_+$ system based on the fact that RI onset would not occur if V hits zero level or becomes negative (i.e., an anticyclonic vortex). We therefore begin with the following lemma that expresses the probability of RI onset occurrence. That is, the probability that V reaches a prescribed level $\ell > 0$ without dying out. Practically, this probability indicates the development of a cyclonic vortex ($v > 0$) instead of anticyclonic vortex ($v < 0$), given that the initial state of the vortex is cyclonic in the Northern hemisphere (or an anticyclonic vortex from an initial anticyclonic state in the Southern Hemisphere).

Lemma III.1 (Probability of RI onset). *Let $p(\mathbf{x}) = \mathbb{P}_{\mathbf{x}}(\tau_+ < \tau_0)$ be the probability of the RI onset occurrence when an initial state of the SDE (6) is $\mathbf{x} = (u, v, b)$. Then, p satisfies the following boundary value problem:*

$$\begin{cases} \mathscr{L}p(\mathbf{x}) = 0 & \text{if } 0 < v < \ell, \\ p(\mathbf{x}) = 1 & \text{if } v = \ell, \\ p(\mathbf{x}) = 0 & \text{if } v = 0, \end{cases} \tag{12}$$

where $\mathscr{L}$ is the operator (11).

Proof 1. The proof is standard and we give a sketch to illustrate the key idea. We recall (7) and (8) and define $\tau := \min\{\tau_+, \tau_0\}$ to be the first time for the v component to exit the interval $(0, \ell)$. Then, the event $\{\tau_+ < \tau_0\}$ is the same as the event $\{V_\tau = \ell\}$ when the starting point $\mathbf{x} = (u, v, b)$ satisfies $v \in [0, \ell]$. Hence, $p(\mathbf{x}) = \mathbb{P}_{\mathbf{x}}(\mathbf{X}_\tau = \ell)$. The random times τ_+, τ_0, and τ are stopping times with respect to the filtration generated by process $\mathbf{X}$. Hence, by the Dynkin's formula (see Ref. 26, Chap. 2)

$$\mathbb{E}_{\mathbf{x}} f(\mathbf{X}_\tau) = f(\mathbf{x}) + \mathbb{E}_{\mathbf{x}}\left[\int_0^\tau \mathscr{L}f(\mathbf{X}_s)\, ds\right], \tag{13}$$

for all bounded functions f in the domain of $\mathscr{L}$. From this and the fact that (12) has unique solution, we can check that p is the solution to (12). □

It should be noted that if the starting point $\mathbf{x}_0 = (u_0, v_0, b_0)$ is fixed (i.e., does not depend on ε) and that $v_0 > 0$, then the probability of RI onset will tend to 1 as $\varepsilon \to 0$. This is because the ODE starting with $v_0 > 0$, which corresponds to the case $\varepsilon = 0$ (i.e., no random fluctuation), always hit level ℓ under the assumption $0 < \ell < v_*$ (i.e., Assumption 1. See also Ref. 22). By Ref. 27 (Lemma 5) and Assumption 1

$$\lim_{\varepsilon \to 0} p(\mathbf{x}_0) = 1 \quad \text{for all } \mathbf{x}_0 = (u_0, v_0, b_0) \in \mathbb{R} \times (0, \ell] \times \mathbb{R}. \tag{14}$$

Physically, this asymptotic behavior of $p(\mathbf{x}_0)$ implies that the probability of RI onset will approach 1 when the random noise effect goes to zero (i.e., $\varepsilon \to 0$) for any initial vortex strength $\mathbf{x}_0$. The validity of this result will be later verified by our Monte Carlo simulation in Sec. IV (cf. Fig. 6).

B. Distribution of RI onset time

We assume that RI onset occurs, the next question one wishes to examine is how the RI onset time τ_+ depends on the model initial conditions or parameters. Answering this question will help forecasters to

estimate the uncertainty of their RI onset prediction as TCs evolve with time.

For this, we start with the Cumulative Distribution Functions (CDF) of τ_+, conditioned on the occurrence of RI onset. Precisely, let $F_{\text{on}}(t,\mathbf{x}) := \mathbb{P}_{\mathbf{x}}(\tau_+ \le t \,|\, \tau_+ < \tau_0)$ be the CDF of τ_+, under the condition that RI onset occurs and the SDE (6) starts from an initial value $\mathbf{x}$. Let $p(\mathbf{x}) = \mathbb{P}_{\mathbf{x}}(\tau_+ < \tau_0)$ be the probability of RI onset as in Lemma III.1, then

$$F_{\text{on}}(t,\mathbf{x}) = \frac{\mathbb{P}_{\mathbf{x}}(\tau_+ \le t\,,\ \tau_+ < \tau_0)}{p(\mathbf{x})}. \tag{15}$$

In Lemma III.2 below, we obtain the numerator of (15) and therefore F_{on}.

Lemma III.2 (Distribution of RI onset time). *Let $G(t,\mathbf{x}) := p(\mathbf{x})\, F_{\text{on}}(t,\mathbf{x}) = \mathbb{P}_{\mathbf{x}}(\tau_+ \le t\,,\ \tau_+ < \tau_0)$. Then, G satisfies the boundary value problem*

$$\frac{\partial G(t,\mathbf{x})}{\partial t} = \mathscr{L}G, \quad t \in (0,\infty),\ \mathbf{x} \in \{(u,v,b) : 0 < v < \ell\}, \tag{16}$$

$$G(0,\mathbf{x}) = 0, \quad \mathbf{x} \in \{(u,v,b)\,:\ 0 < v < \ell\}, \tag{17}$$

$$G(t,\mathbf{x}) = 0, \quad t \in (0,\infty),\ \mathbf{x} \in \{(u,0,b),\ (u,\ell,b)\}, \tag{18}$$

where $\mathscr{L}$ is the operator (11).

Proof 2. The initial condition (17) and the boundary condition (18) are clearly satisfied. Let $H(t,\mathbf{x}) := \mathbb{P}_{\mathbf{x}}(\tau_+ > t\,,\ \tau_+ < \tau_0) = p(\mathbf{x}) - F_{\text{on}}(t,\mathbf{x})$.

Let $\mathbf{X}^{ab}$ be the absorbed diffusion[28] obtained when $\mathbf{X}$, the solution to SDE (6), is absorbed upon hitting the boundary of the domain $D = \{(u,v,b)\,:\ 0 < v < \ell\}$. By the strong Markov property of $\mathbf{X}^{ab}$

$$\begin{aligned} H(t,\mathbf{x}) &= \mathbb{P}_{\mathbf{x}}(\mathbf{X}^{ab}_t \in D,\ \tau_+ < \tau_0) \\ &= \int_D \mathbb{P}_{\mathbf{y}}(\tau_+ < \tau_0)\, \mathbb{P}_{\mathbf{x}}(\mathbf{X}^{ab}_t \in d\mathbf{y}) \\ &= \int_D p(\mathbf{y})\, p^{ab}(t,\mathbf{x},\mathbf{y})\, d\mathbf{y}, \end{aligned}$$

where $p^{ab}(t,\mathbf{x},\mathbf{y})$ is the transition density of X^{ab}. By the backward Kolmogorov's inequality (Ref. 25, Chap. 5), we have $\frac{\partial H(t,\mathbf{x})}{\partial t} = \mathscr{L}H(t,\mathbf{x})$ and hence (16). □

Unlike Theorem III.1 that focuses on whether or not an RI onset would occur, Lemma III.2 informs us the probability of having an RI onset time no later than a given time t if the initial condition is $\mathbf{x} = (u,v,b)$. We note that one can always numerically solve (16)–(18) to obtain $F_{\text{on}}(t,\mathbf{x})$. We can then verify Lemma III.2 by comparing the corresponding probability density function (i.e., its time-derivative $\frac{\partial F_{\text{on}}}{\partial t}$) with the histograms of RI onset statistics obtained from the Monte Carlo simulation of the MSD system (3) (cf. Fig. 6).

To obtain more quantitative insight about τ_+, we establish in Theorem III.3 below the limiting distribution of the onset time probability density distribution for τ_+ as $\varepsilon \to 0$. Let $[u(t), v(t), b(t)]_{t\ge 0}$ be the solution of the ODE (3) starting at $\mathbf{x}_0 = (u_0, v_0, b_0)$ and $T = \inf\{t \ge 0\,;\, v(t) = \ell\}$, we then have

Theorem III.3 (Asymptotic distribution of RI onset time). *We suppose the initial state of the SDE (6) is the same as that of the ODE (3); that is, $\mathbf{X}_0 = \mathbf{x}_0 = (u_0, v_0, b_0)$. We suppose $v_0 \in (0,\ell)$ and that the onset level ℓ satisfies Assumption 1. Then, as $\varepsilon \to 0$, the random variable $\varepsilon^{-1}(\tau_+ - T)$ converges in distribution to the centered Gaussian random variable with variance*

$$\frac{\Sigma_{22}(T)}{\ell^2\,[u(T)+\ell]^2}, \tag{19}$$

where $\Sigma(t) = [\Sigma_{ij}(t)]$ is the 3×3 matrix

$$\Sigma(t) = e^{\int_0^t A(r)dr} \cdot \left(\int_0^t e^{-\int_0^s A(r)dr} e^{-\int_0^s A^\top(r)dr}\, ds \right) \cdot e^{\int_0^t A^\top(r)dr}, \tag{20}$$

and $A(t) = A_{\mathbf{x}_0}(t)$ is the Jacobian matrix $\nabla\mu(\mathbf{x}(t))$, that is,

$$A(t) = \begin{pmatrix} -v(t) & 2p\,v(t) - u(t) & -(p+1) \\ -v(t) & -u(t) - 2v(t) & 0 \\ b(t)+s & 1 & u(t) - r \end{pmatrix}. \tag{21}$$

An immediate consequence of Theorem III.3 is an asymptotic formula for the variance of τ_+, conditioned on RI onset occurrence (τ_+ is infinity by convention if RI does not occur, so we should consider the conditional variance rather than the variance of τ_+).

Corollary 1 (Variance of RI onset time). *As $\varepsilon \to 0$, the distribution of the RI onset time τ_+ is well approximated by a Gaussian variable with mean T and conditional variance*

$$Var(\tau_+ \,|\, \tau_+ < \tau_0) \approx \varepsilon^2\, \frac{\Sigma_{22}(T)}{\ell^2\,[u(T)+\ell]^2}. \tag{22}$$

Corollary 1 is noteworthy because it captures the behavior of the conditional variance of the RI onset timing τ_+ in terms of the initial condition $\mathbf{x}_0$ as well as the model parameters p, r, s as $\varepsilon \to 0$, which is proportional to the variance of the additive noise ε^2. For practical applications, this explicit dependence of the variability of RI onset timing on model parameters or initial condition allows one to quantify how the uncertainty of RI onset forecast changes when a TC evolves or ambient environment varies. As will later be verified in our numerical simulations, examination of its dependence on the model parameters (p, r, s) shows that the probability distribution for τ_+ is close to a Gaussian distribution centered at T when $\varepsilon \to 0$ as proven in Corollary 1.

Proof 3 (Proof of Theorem III.3). *Our proof is based on Theorem 1 in Ref. 27 which gives an asymptotic result for a small noise stochastic diffusion equation*

$$dX_\varepsilon(t) = [\mu(X_\varepsilon(t)) + \varepsilon^{\alpha_1}\Psi_\varepsilon(X_\varepsilon(t))]dt + \varepsilon\sigma(X_\varepsilon(t))dW_t, \tag{23}$$

$$X_\varepsilon(0) = \mathbf{x}_0 + \varepsilon^{\alpha_2}\xi_\varepsilon. \tag{24}$$

We need to check the conditions of that theorem before we can apply it. By taking $\xi_\varepsilon \equiv 0$, $\Psi_\varepsilon \equiv 0$, $\alpha_1 = 1$, and $\sigma(\cdot) = I_{3\times 3}$ the unit matrix in (23) and (24), we obtain (5), with the unperturbed initial condition $\mathbf{X}_0 = \mathbf{x}_0$. We let M be the hyperplane $M = \{(u,v,b) \in \mathbb{R}^3 : v = \ell\}$ in $\mathbb{R}^3$. Then, the hitting time τ_ε in Theorem 1 of Ref. 27 is exactly the RI onset time τ_+ defined in (7).

Step 1: Joint convergence. *We recall that the deterministic time T defined by (10) is the first time the trajectory v of the ODE (2) hits level ℓ. We denote by $z := (z_1, z_2, z_3) = [u(T), \ell, b(T)]$ the point where the trajectory of the MSD system (3) hits M. In Ref. 29, it is assumed that the deterministic vector field μ is smooth, and the*

deterministic time defined by (10) must satisfy $0 < T < \infty$. *Moreover, it is assumed that* $\mu(z)$ *does not belong to the tangent space* T_{zM} *of* M *at the point* z *(or in other words the orbit of the system (3) intersects* M *and the crossing is transversal). These assumptions are satisfied by our MSD system (3) under Assumption 1. Therefore, we can indeed apply Theorem 1 of Ref. 27.*

Let π_μ *be the projection onto span*$[\mu(z)]$ *along* T_{zM} *and* π_M *the projection onto* T_{zM} *along span*$[\mu(z)]$; *see Fig. 3. Then for any vector* $\eta \in \mathbb{R}^3$, $\pi_\mu\eta \in \mathbb{R}$ *and* $\pi_M\eta \in T_zM$ *satisfy*

$$\eta = \pi_\mu\eta \cdot \mu(z) + \pi_M\eta.$$

Note that in our case, the tangent space T_{zM} *is exactly* M *itself since it is a plane. Theorem 1 of Ref. 27 asserts the following convergence in distribution as* $\varepsilon \to 0$:

$$\varepsilon^{-1}(\tau_+ - T,\, X_\varepsilon(\tau_+) - z) \xrightarrow{d} \big(-\pi_\mu\phi_0(T), \pi_M\phi_0(T)\big), \tag{25}$$

where

$$\phi_0(t) = \Phi_{\mathbf{x}_0}(t) \int_0^t \Phi_{\mathbf{x}_0}(s)^{-1}\, dW(s) \tag{26}$$

is a random vector in $\mathbb{R}^3$. *The matrix-valued function* $\Phi_{\mathbf{x}_0}(t) = e^{\int_0^t A_{\mathbf{x}_0}(r)dr}$ *solves the equation*

$$\frac{d}{dt}\Phi_{\mathbf{x}_0}(t) = A_{\mathbf{x}_0}(t)\Phi_{\mathbf{x}_0}(t),$$
$$\Phi_{\mathbf{x}_0}(0) = I_{3\times 3},$$

where $A_{\mathbf{x}_0}(t)$ *is* given *by (21).*

Step 2: Projection and variance computation. *The above 3-dimensional random vector (26) is Gaussian distributed with mean zero and co-variance matrix* $\Sigma(t)$ *given by (20). That is,* $\phi_0(t) \sim \mathcal{N}[0, \Sigma(t)]$. *Let* $\phi_0(T) = [\phi_{0,1}(T), \phi_{0,2}(T), \phi_{0,3}(T)]$. *Clearly,* $\phi_{0,2}(T) \sim \mathcal{N}[0, \Sigma_{22}(T)]$.

By definition of the projections, we have

$$\phi_0(T) = \pi_\mu\phi_0(T)\mu(z) + \pi_M\phi_0(T),$$

where $\pi_\mu\phi_0(T) \in \mathbb{R}$ *and* $\pi_M\phi_0(T) \in T_zM$. *See Fig. 3 with* $\eta = \phi_0(T)$ *for an illustration. Since* T_{zM} *is parallel to the (u, b)-plane, the second coordinate (i.e., the v-coordinate) of* $\phi_0(T)$ *is the same as that of* $\pi_\mu\phi_0(T)\mu(z)$. *That is,*

$$\phi_{0,2}(T) = \pi_\mu\phi_0(T) \cdot \mu_2(z).$$

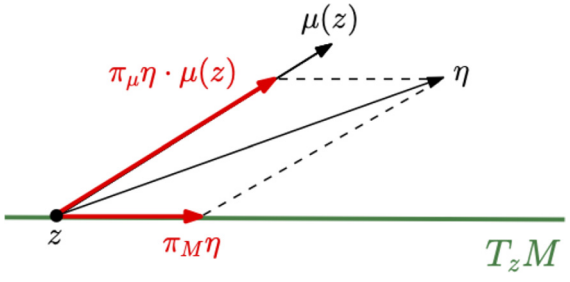

FIG. 3. Illustration of the projections $\pi_\mu\eta \in \mathbb{R}$ and $\pi_M\eta \in T_zM$. Given vectors η, $\mu(z) \in \mathbb{R}^3$ and the tangent plane T_{zM}, we have $\eta = \pi_\mu\eta \cdot \mu(z) + \pi_M\eta$.

This implies that

$$\pi_\mu\phi_0(T) = \frac{\phi_{0,2}(T)}{\mu_2(z)}, \tag{27}$$

and so $\pi_\mu\phi_0(T)$ is a centered Gaussian vector with variance $\frac{\Sigma_{22}(T)}{\mu_2(z)^2}$.

Step 3: Conclusion. *In conclusion, from (25), for* ε *close to zero we get that in distribution*

$$(\tau_+, X_\varepsilon(\tau_+)) \approx (T, z) + \varepsilon(-\pi_\mu\phi_0(T), \pi_M\phi_0(T)). \tag{28}$$

From (28) and (14), the conditional expectation

$$\mathbb{E}_{\mathbf{x}_0}[\tau_+ \,|\, \tau_+ < \tau_0] \to T \text{ as } \varepsilon \to 0, \tag{29}$$

because $\phi_0(T)$ *is a centered Gaussian vector. For the conditional variance*

$$Var(\tau_+ \,|\, \tau_+ < \tau_0) \approx \varepsilon^2 \frac{\Sigma_{22}(T)}{\mu_2(z)^2} = \varepsilon^2 \frac{\Sigma_{22}(T)}{z_2^2(z_1 + z_2)^2}.$$

□

C. Hitting analysis for one-dimensional reduction

The typical behavior of TC dynamics shown in Fig. 1 captures an important characteristic of TC development. Specifically, the pre-RI period before TC intensity rapidly amplifies is characterized by very slow evolution, much like a constant-forcing dynamical system. One can therefore exploit this property to further study RI onset by reducing the MSD system to a general one-dimensional SDE model for the v component, which can provide additional insights into the variability of RI onset time. That is, we wish to examine herein a particular case in which *the noise* ε *is fixed while* v_0 *is small* ($v_0 \to 0$). This case differs from (14) and Theorem III.3, which focus on the probability of RI onset and the distribution of the onset time for a limit of the small noise $\varepsilon \to 0$ with a fixed initial condition v_0. As such, the behaviors of RI onset for a fixed noise ε but small v_0 are unclear from Theorem III.3 that we wish to examine in this subsection.

For this purpose, we observe from our Monte Carlo simulations of the MSD system to be presented in Sec. IV that (see the lower left panels in Fig. 6)

- $\mathcal{O}1$: the probability of RI onset gets smaller as $v_0 \to 0$.
- $\mathcal{O}2$: the conditional distribution of the RI onset time τ_+ (given that an RI onset occurred) is skewed to the left and has a *smaller* averaged value than the deterministic onset time T.

This regime (i.e., v_0 is very small compared with ε) is challenging to analyze, because a standard Gaussian approximation is no longer valid. However, it is possible to offer some insight into the aforementioned observations through the following general 1-dimensional SDE:

$$dZ_t = F(Z_t)\, dt + \varepsilon dW_t, \tag{30}$$

where W is the Wiener process in $\mathbb{R}$, and $F : \mathbb{R} \to \mathbb{R}_+$ is an arbitrary given smooth function such that

$$F(0) = 0 \quad \text{and} \quad F(x) > 0 \text{ for } x > 0. \tag{31}$$

Our aim here is to compare the qualitative behavior of the V-component of (6) and the process Z solving (30), when the initial value v_0 is "small."

How "small" the initial value is depends on the fixed noise level ε, as quantified in Theorem III.5 below.

Remark 2. It is natural to question why one wishes to further examine a 1-dimensional SDE, given that the condition of TC initial intensity v_0 less than the noise amplitude ε is not realized in reality. We should emphasize here, however, that it is not our intention to applying (30) to real TC development. Instead, the aim of this 1D system is to qualitatively capture the behaviors of TC dynamics during the initial development up to the RI onset moment for which the MSD forcing can be approximated as a constant. The advantage of this 1D analysis lies in the fact that the forcing function F can now be quite general; that is, we do not require any specific functional form for F. Thus, our analysis for the 1D system (30) works for a larger class of forcing functions F.

We consider the hitting times at the endpoints 0 and ℓ. That is,

$$\tau_i := \inf\{t \geq 0 : Z_t = i\} \quad \text{for } i = 0, \ell.$$

Analogous to the probability of RI onset is $\mathbb{P}_{\mathbf{x}}(\tau_\ell < \tau_0)$, the probability of hitting ℓ before 0 provided that (30) starts at $Z_0 = x$. Lemma III.4 below gives an exact formula for this, which is not available in higher dimensions in general.

Lemma III.4. *The probability of hitting ℓ before 0 for Z in (30) starting at $x \in [0, \ell]$ is*

$$\mathbb{P}_x(\tau_\ell < \tau_0) = \frac{\int_0^x k_\varepsilon(y)\, dy}{\int_0^\ell k_\varepsilon(y)\, dy},$$

where k_ε is the function

$$k_\varepsilon(y) = \exp\left\{\frac{-2}{\varepsilon^2}\int_0^y F(t)dt\right\}. \tag{32}$$

The following result quantifies a dichotomy for the probability $\mathbb{P}_{\varepsilon^\alpha}(\tau_\ell < \tau_0)$ of hitting ℓ before 0, starting at ε^α. Namely, this probability is close to 0 if the starting point is small (α large), and close to 1 when the starting point is large (α small).

Theorem III.5 (Asymptotic hitting probability). *We suppose F is a smooth function satisfying (31) and $F'(0) > 0$. For all $c > 0$, the probability of hitting ℓ before 0 for Z in (30) starting at $c\,\varepsilon^\alpha$ satisfies*

$$\lim_{\varepsilon\to 0}\mathbb{P}_{c\varepsilon^\alpha}(\tau_\ell < \tau_0) = \begin{cases} 1 & \text{if } \alpha \in (0,1), \quad \text{i.e., starting point is not small,} \\ erf\left(c\sqrt{F'(0)}\right) & \text{if } \alpha = 1, \\ 0 & \text{if } \alpha > 1, \quad \text{i.e., starting point is very small,} \end{cases}$$

where $erf(x) := \frac{2}{\sqrt{\pi}}\int_0^x e^{-z^2}\, dz$ is the error function.

Remark 3. Analogous to the RI onset indicator (44) is the inverse $h_\varepsilon^{-1}(0,8)$ where $h_\varepsilon(z) = \mathbb{P}_z(\tau_\ell < \tau_0)$. From the critical case $\alpha = 1$, for $\varepsilon \approx 0$, we have $h_\varepsilon(z) = erf\left(\frac{z}{\varepsilon}\sqrt{F'(0)}\right)$. Then

$$h_\varepsilon^{-1}(0.8) \approx \frac{\varepsilon}{\sqrt{F'(0)}}\, erf^{-1}(0.8)$$

is linear in ε when $\varepsilon \approx 0$. This is consistent with the approximately linear curve in Fig. 5.

Now we condition on the event $\{\tau_\ell < \tau_0\}$ and consider the conditional distribution of the hitting time τ_ℓ. We shall compute conditional expected time. This is analogous to conditioning on RI onset occurrence and consider the conditional distribution of the RI onset time. Precisely, we shall compute the conditional expected time

$$\mathbb{E}_x[\tau_\ell \,|\, \tau_\ell < \tau_0]. \tag{33}$$

For the rest of this section, we obtain an explicit formula for this conditional expected time in Lemma III.6 and study its asymptotic behavior in Theorem III.7 below.

Lemma III.6. *For $x \in (0, \ell]$,*

$$\mathbb{E}_x[\tau \,|\, \tau_\ell < \tau_0] = \frac{2}{\varepsilon^2}\frac{1}{\int_0^x k_\varepsilon(z)dz}\left\{\int_x^\ell\int_0^x k_\varepsilon(z)k_\varepsilon(u)\int_u^z \frac{p(y)}{k_\varepsilon(y)}\, dy\, du\, dz\right\}, \tag{34}$$

where $p(\mathbf{x}) = \mathbb{P}_{\mathbf{x}}(\tau_\ell < \tau_0)$ is the probability in Lemma III.4.

Theorem III.7 below asserts that as the starting point $x \to 0$

$$\mathbb{E}_x[\tau_\ell \,|\, \tau_\ell < \tau_0] \approx \Psi(\varepsilon) - \frac{x^2}{3\varepsilon^2}, \tag{35}$$

for some positive number $\Psi(\varepsilon)$.

Theorem III.7 (Asymptotic conditional hitting time). *We suppose F is a continuous function. For each fixed noise level $\varepsilon > 0$*

$$\lim_{x\to 0}\mathbb{E}_x[\tau_\ell \,|\, \tau_\ell < \tau_0] = \Psi(\varepsilon), \tag{36}$$

where

$$\Psi(\varepsilon) = \frac{2}{\varepsilon^2}\int_0^\ell k_\varepsilon(u)\int_0^u \frac{p(y)}{k_\varepsilon(y)}\, dy\, du \in (0,\infty). \tag{37}$$

Furthermore, we suppose F satisfies (31) and $F'(0) > 0$. Then,

$$\lim_{x\to 0}\frac{\Psi(\varepsilon) - \mathbb{E}_x[\tau_\ell \,|\, \tau_\ell < \tau_0]}{x^2} = \frac{1}{3\varepsilon^2}. \tag{38}$$

Theorem III.7 implies that, fixing a noise level $\varepsilon > 0$, the conditional expected hitting time $\mathbb{E}_x[\tau_\ell \,|\, \tau_\ell < \tau_0]$ stays bounded as $x \to 0$. This is in contrast to the deterministic analogue [which tends to infinity in the order of $O(-\log x)$ as $x \to 0$ when $F'(0) > 0$]. Since

$$\Psi(\varepsilon) - \frac{x^2}{3\varepsilon^2} \ll O(-\log x) \quad \text{as } x \to 0. \tag{39}$$

Theorem III.7 provides a possible explanation to the observation that the conditional expected hitting time is *shorter* than the deterministic hitting time, mentioned in observation $\mathcal{O}2$ at the beginning of this section.

IV. NUMERICAL RESULTS

A. Algorithm

From the practical standpoint, Lemma III.1, Lemma III.2, and Theorem III.3 presented in Sec. III are useful for RI forecast applications, because they directly indicate the probability of RI onset occurrence as well as the variability of RI onset time. In this section, we will present numerical investigation to validate a number of theoretical results presented in Sec. III, from which further examination of RI onset on various model parameters and initial conditions can be

obtained. In particular, we wish to verify the variance formula (20) in Corollary 1 for RI onset time because of its importance in real-time forecast. While this formal variance expression is mathematically significant, we note that its direct calculation is challenging because of the matrix exponent and integration that are sensitive to matrix operations. As such, we present in this section a numerical algorithm to compute the matrix $\Sigma(t)$ efficiently.

For the numerical purposes, we observe that the variance matrix $\Sigma(t)$, defined in (20), solves the following differential equation:

$$\frac{d\Sigma(t)}{dt} = I_{3\times 3} + A_{\mathbf{x}_0}(t)\Sigma(t) + \Sigma(t)A_{\mathbf{x}_0}(t)^\top, \tag{40}$$

where the matrix $A_{\mathbf{x}_0}(t)$ is defined in (21). The above Eq. (40) can be indeed derived by rewriting

$$\Sigma(t) = \Phi_{\mathbf{x}_0}(t)\cdot N(t)\cdot(\Phi_{\mathbf{x}_0}(t))^\top, \tag{41}$$

where $N(t) = (\int_0^t \Phi_{\mathbf{x}_0}(s)^{-1}(\Phi_{\mathbf{x}_0}(s)^{-1})^\top\, ds)$, and $\Phi_{\mathbf{x}_0}(t)$ is the solution of the following differential equation:[27]

$$\frac{d}{dt}\Phi_{\mathbf{x}_0}(t) = A_{\mathbf{x}_0}(t)\Phi_{\mathbf{x}_0}(t),$$
$$\Phi_{\mathbf{x}_0}(0) = I_{3\times 3}.$$

After taking derivatives in (41) and applying the product rule, we get

$$\frac{d}{dt}\Sigma(t) = \frac{d}{dt}\Phi_{\mathbf{x}_0}(t)\cdot N(t)\cdot(\Phi_{\mathbf{x}_0}(t))^\top + \Phi_{\mathbf{x}_0}(t)\cdot\frac{d}{dt}N(t)\cdot(\Phi_{\mathbf{x}_0}(t))^\top + \Phi_{\mathbf{x}_0}(t)\cdot N(t)\cdot\frac{d}{dt}(\Phi_{\mathbf{x}_0}(t))^\top. \tag{42}$$

By Sec. IV A and the fact that $\frac{d}{dt}N(t) = \Phi_{\mathbf{x}_0}(t)^{-1}(\Phi_{\mathbf{x}_0}(t)^{-1})^\top$, we thus have

$$\frac{d}{dt}\Sigma = A_{\mathbf{x}_0}\Phi_{\mathbf{x}_0}N\Phi_{\mathbf{x}_0}^\top + \Phi_{\mathbf{x}_0}\Phi_{\mathbf{x}_0}^{-1}(\Phi_{\mathbf{x}_0}^{-1})^\top\Phi_{\mathbf{x}_0}^\top + \Phi_{\mathbf{x}_0}N\Phi_{\mathbf{x}_0}^\top A_{\mathbf{x}_0}^\top. \tag{43}$$

Using (41) again and rearranging the right-hand side of Eq. (43), we thus obtain Eq. (40) for the variance matrix $\Sigma(t)$.

The particular benefit of this differential equation approach for $\Sigma(t)$ instead of the formula (20) in Corollary 1 is that it allows for integrating the matrix equation (40) forwards in time from any initial condition up to any given time t without the need of explicitly computing the exponent of matrix integration in Eq. (20). We note, however, that this algorithm requires computing the coefficient matrix $A(t)$ along the trajectory, which is the Jacobian matrix of the model state as seen in Eq. (21). As a result, we have to integrate the deterministic model (1) first and store the entire trajectory $[u(t), v(t), b(t)]$ before the integration of (40) can be carried out.

Along with the above numerical algorithm to obtain the variance formula in Corollary 1, Monte Carlo simulations of the MSD model (6) will be also carried out to verify Corollary 1. For these Monte Carlo simulations, the MSD system (6) is integrated by using the Runge–Kutta fourth-order scheme with time step $dt = 0.001$. As mentioned in Ref. 7, the stochastic forcing in the MSD system (6) is additive with no state dependence. Thus, the Runge–Kutta scheme can be applied to the deterministic part of Eq. (6), with the stochastic forcing added at each time step. This method retains the fourth-order accuracy for the deterministic part, while the stochastic accuracy order first orders as for the Euler–Maruyama scheme.[30]

Because of the random nature of stochastic forcing, all Monte Carlo simulations in this study are carried out with 1000 realizations for each choice of initial conditions and random forcing amplitude ε. A fixed set of parameters for the MSD model with $(p, r, s) = (200, 0.25, 0.1)$ similar to those used in Ref. 7 is also employed in all simulations. These parameters are typical for TCs in real atmospheric conditions as shown in Refs. 23 and 7. By comparing the results from the numerical integration of Eq. (40) and the Monte Carlo simulations of the MSD system, the validity of the theoretical results in Sec. III can be assessed.

B. RI onset probability

We investigate first in this subsection the probability of RI onset occurrence as presented in Lemma III.1, using the Monte Carlo simulations of the MSD system. These Monte Carlo simulations will serve as a reference from which one can validate the theoretical results obtained in Sec. III.

Figure 4(a) shows the probability on RI onset $p(u_0, v_0, b_0)$ as a function of the initial condition v_0. Consistent with observations,[31] one notices that the RI occurrence probability quickly increases with v_0, regardless of the random forcing amplitude ε. For $\varepsilon < 10^{-2}$, the RI occurrence probability reaches the value of $\sim$1 for all $v_0 > 0.05$. This means RI will be almost guaranteed to occur, because a sufficiently strong initial vortex would practically mean that a TC is well organized and so it will most likely undergo RI.

As the random fluctuation increases ($\varepsilon > 0.03$), one notices however that the probability for RI occurrence increases slower and approaches 1 only when v_0 is sufficiently large (>0.1). This threshold justifies the hereinafter use of $\ell = 0.1$ for RI onset time in the MSD system (this level 0.1 for v_0 in the non-dimensional unit corresponds to $\sim$10 ms^{-1} in full physical dimension. See, e.g., Refs. 17 and 32).

Given the strong dependence of TC development on ambient environment, it is thus expected that the RI onset probability should be governed by not only initial conditions but also environmental factors. Among the three model parameters (p, r, s), we note that s is most sensitive to ambient environment because it represents the stratification of the troposphere.[22,23] Thus, Fig. 4(b) shows the dependence of RI probability as a function of s with fixed values for $\varepsilon = 0.01$, $v_0 = 0.02$ and all other parameters. Consistent with the previous studies on weaker intensity for more stable troposphere,[33–39] one notices in Fig. 4(b) that RI onset probability decreases quickly as s is larger (i.e., the troposphere becomes more stable). Given the same initial vortex strength, an increase in s from 0.1 to 0.2 could reduce the RI onset probability from 80% to 60%, which is substantial in operational forecast. For smaller values of v_0, this drop in RI onset probability is even much faster, suggesting that the environmental static stability is a key parameter not only for the TC maximum intensity but also for RI onset prediction.

A different way to examine the sensitivity of RI onset probability in operational practice is to determine what value of the initial TC strength v_0 would allow for at least, for example, 80% RI probability as a function of the random magnitude ε. This 80% threshold is generally sufficient for most practical purposes to ensure that RI onset will be very likely to occur, from which timely risk management can be prepared. In this regard, Fig. 5 shows the minimum initial TC strength I_0^ε to meet the 80% RI onset probability threshold as a function of ε. Here, we define I_0^ε, which can be considered as an RI onset indicator, as the unique number within $(0, \ell)$ such that

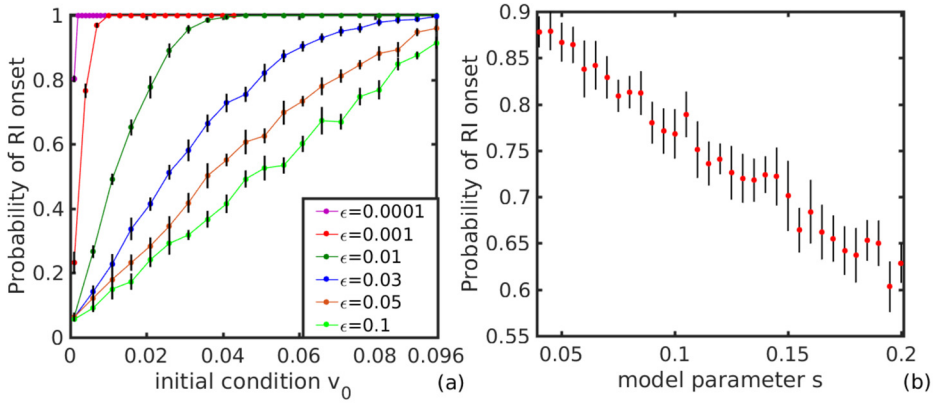

FIG. 4. (a) Probability of RI onset as a function of the initial wind component v_0, with different values of ε and $s = 0.1$; and (b) probability of RI onset as a function of s, where $v_0 = 0.02$ and $\varepsilon = 0.01$. In both figures, other parameters are $(p, r) = (200, 0.25)$ and $(u_0, b_0) = (-0.01, 0.0001)$. All error bars with a 95% confidence interval are obtained by bootstrapping the sample.

$$p(u_0, I_0^\varepsilon, b_0) = 0.8. \tag{44}$$

Consistent with our theoretical results, I_0^ε increases linearly with ε when ε is small. It also appears that I_0^ε levels off for $\varepsilon > 0.07$. The limit of a small ε is of interest, as it reveals that the MSD system behaves similarly to a one-dimensional stochastic system with autonomous forcing as presented in Sec. III C. As explained in Remark 3, Theorem III.5 shows that the linear dependence of I_0^ε on ε is always valid for a very general one-dimensional system, so long as the forcing does not vary much prior to RI onset. This is applied well to the MSD system as seen, for example, in Fig. 1, which shows that TCs evolve very slowly during the pre-RI onset period. Physically, this result thus confirms that larger random noise would require stronger initial intensity so that RI onset can be more likely to occur. Note that when the initial intensity is sufficiently large, random noise will have less of an impact because RI onset will almost guarantee to occur (at a 80% level) for those initially strong intensity states. Despite its simplification, it is apparent that the MSD system could capture well several key properties of RI onset probability as shown in Fig. 4. This indicates that the TC-scale framework is useful for studying TC development, and can be used to further examine the variability of RI onset timing in Sec. IV C.

C. RI onset timing variability

Given the probability of RI onset occurrence as presented in Sec. IV B, we wish to verify next the distribution of RI onset time as given by Theorem III.3 and related Corollary 1. Because RI onset is almost guaranteed to occur when v_0 is sufficiently large as shown in Fig. 5, we will consider here a specific case in which the hitting level ℓ for RI onset (i.e., v component) is $\ell = 0.1$.

Similar to Sec. IV B, our main focus herein will be again on how the distribution of τ_+ changes with the initial condition for the v component (i.e., v_0), while keeping the other two components (u_0, b_0) fixed at the same values of $u_0 = -10^{-2}$, $b_0 = 10^{-4}$. This is because v_0 practically represents the initial intensity of a TC vortex during its early stage of development. During this tropical disturbance stage, there is no strong dynamical constraint among the TC scales and one can therefore assign relatively independent values for u_0, v_0, b_0. As a tropical disturbance grows, its dynamics will be, however, governed by the TC-scale dynamics and they can no longer evolve independently.

To have a broad picture of the variability of RI onset time, Fig. 6 shows the histograms of τ_+ for a range of v_0 and ε. Here, these histograms are constructed from 1000 Monte Carlo simulations, using the default values for the parameters and initial conditions as mentioned in Sec. IV A. One notices in Fig. 6 an expected behavior of the τ_+ variability, with a narrower distribution of τ_+ for smaller ε when $v_0 \geq 0.01$. That is, a smaller random forcing would result in less variability in RI onset timing, which is consistent with real TC development.

Of further interest from Fig. 6 is that for each fixed initial condition v_0 (i.e., for each row), the conditional distribution of τ_+ gets closer to a probability density function centered around the deterministic onset time T defined in (10) as $\varepsilon \to 0$. This indicates that the

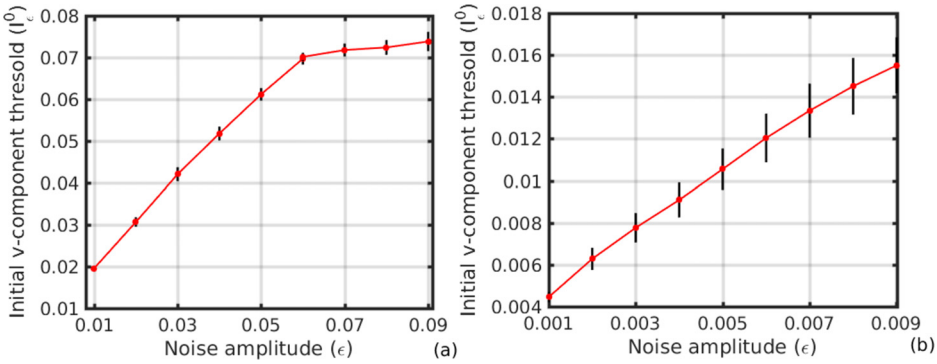

FIG. 5. Dependence of the smallest value of v_0 at which the probability of RI onset reaches a 0.8 level, denoted as I_0^ε defined in (44), on different ranges of the noise level ε including (a) $\varepsilon \in [0 - 0.1]$, and (b) a zoom in for $\varepsilon \in [0.001 - 0.01]$. Other parameter settings include $(p, r, s) = (200, 0.25, 0.1)$ and $u_0 = -0.01$, $b_0 = 0.0001$.

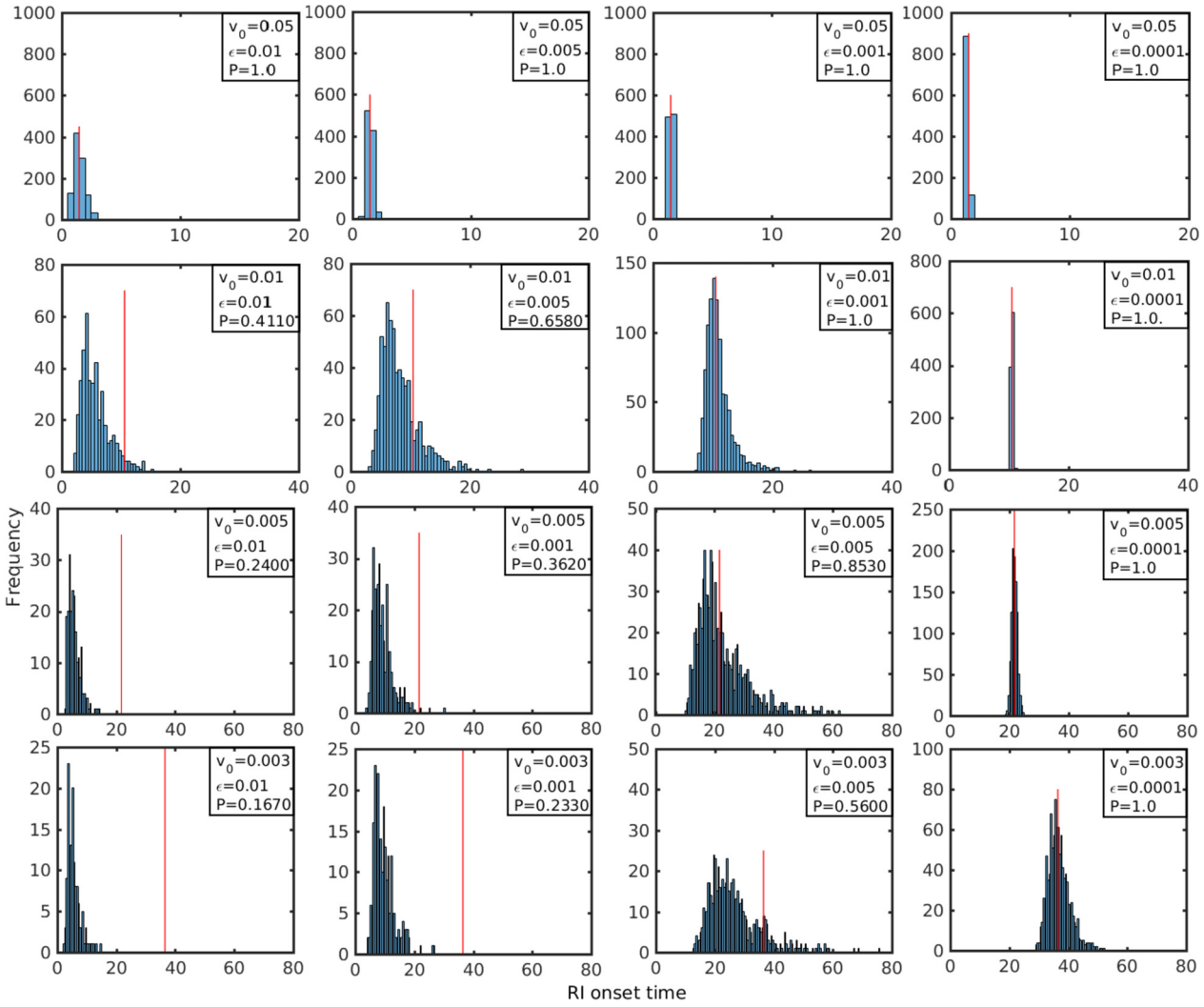

FIG. 6. Histograms of RI onset time τ_+ defined in (7) for various values of initial conditions v_0 and the noise amplitude ε, conditioned on the event $\{\tau_+ < \tau_0\}$. We note that for each 1000-realization set of the stochastic system (6), only a fraction P of them hit $\{v = 0.1\}$ before hitting $\{v = 0\}$ and so only these trajectories are counted (these probability values P are given in the upper right boxes). The red vertical line shows the time T, defined in (10), obtained from the deterministic MSD system as $v(t)$ hits level $v = 0.1$. In all histograms, the parameters are $p = 200$, $r = 0.25$, $s = 0.1$, and the initial values are $u_0 = -0.01$, $b_0 = 0.0001$ used.

deterministic RI onset forecast will be more reliable for either smaller stochastic noises or stronger initial intensity.

For very small values of v_0 (i.e., weaker initial intensity), the center of the τ_+ distribution is shifted farther away from the deterministic time T as ε increases (see the lower left panels in Fig. 6). This is because random fluctuation, which is proportional to ε, is now much larger than the initial condition that TC development is no longer determined by v_0. Instead, the variability of RI onset time τ_+ is more a result of the random noise amplitude ε alone, so long as $v_0 \ll \varepsilon \ll 1$, the TC initial condition becomes irrelevant to RI onset. This characteristic of RI onset timing uncertainty is also consistent with the probability of RI onset occurrence shown in Fig. 6 (see the RI onset probability P in the upper right boxes).

From the mathematical perspective, the behavior of RI onset time for the limit of small v_0 can be also understood by using the general one-dimensional SDE model presented in Sec. III C. As long as TC dynamics evolves slowly prior to RI onset, one can in fact obtain an exact dependence of the center of the τ_+ histogram on ε in terms of the stochastic conditioned diffusion process (see Lemma 2). That is, the random noise in the MSD system induces a modified drift along the gradient of probability density, which results in a faster approach to the ℓ level as shown in Fig. 6. Thus, a smaller value of v_0 (i.e., weaker initial vortex) indicates less likely for RI onset to occur. For ε that is sufficiently larger than v_0, the probability P for RI onset occurrence is quickly reduced below 50%, regardless of value of v_0 (see lower left panels in Fig. 6).

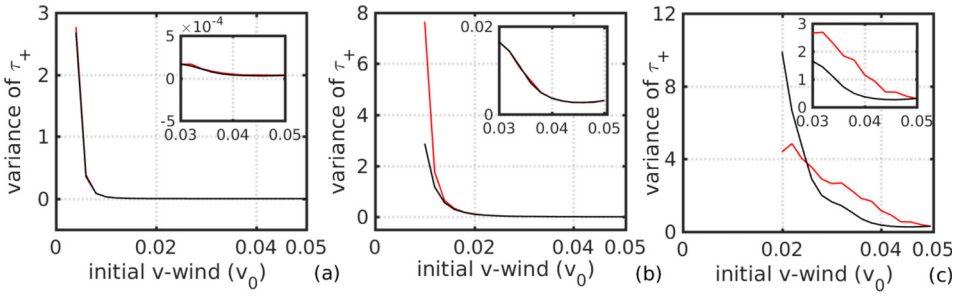

FIG. 7. (a) A diagram shows the variance of the RI onset time τ_+ conditioned on RI onset occurrence as a function of v_0 for noise $\varepsilon = 10^{-4}$, which is obtained from Corollary 1 (black) and from Monte Carlo simulation (red). (b) and (c) Similar to (a) but for $\varepsilon = 10^{-3}$, and $\varepsilon = 10^{-2}$. Upper right corner panels show the zoom in of these $Var(\tau_+|\tau_+ < \tau_0)$ values for $v_0 \in [0.03 - 0.05]$.

To facilitate our comparison of the above results obtained from the Monte Carlo simulations with Theorem III.3, the dependence of the variance of RI onset time on v_0 for each value of ε is summarized in Fig. 7. Consistent with that shown in Fig. 6, the variance of τ_+ decreases with v_0 for all range of ε as expected. We note that the conditional variance of τ_+ (conditioned on occurrence of RI onset) also increases as ε increases, suggesting larger variability of RI onset time when the amplitude of random forcing increases.

Comparing to the conditional variance of τ_+ obtained from Corollary 1 using the numerical integration of Eq. (43) (see the black curves in Fig. 7), it is evident that Corollary 1 could capture consistent characteristics of the conditional variance of τ_+ as a function of ε. This is especially true when ε is much smaller than v_0 [Figs. 7(a) and 7(b)], which shows a good match between Corollary 1 and the Monte Carlo simulations. For $\varepsilon \geq 0.01$, Corollary 1 starts to diverge from the Monte Carlo simulations [Fig. 7(c)], as it tends to underestimate the conditional variance of τ_+ when v_0 increases. In this regard, the Monte Carlo simulations not only confirm the validity of Corollary 1 for a small limit of $\varepsilon \leq 10^{-3}$, but also give us the range of random noise that our theoretical estimation could provide the most reliable dependence of $Var(\tau_+ \,|\, \tau_+ < \tau_0)$ on v_0.

From the application standpoint, the fact that the variability of RI onset timing decreases rapidly for initially stronger intensity (i.e., a larger value of v_0) would suggest that our ability to predict RI onset will be improved as TCs become stronger. This accords with previous observational and modeling studies,[31,40] which showed indeed an overall improved RI forecast as TCs become more organized. Therefore, Theorem III.3 is anticipated and will be useful for further examination of the dependence of τ_+ as well as its variance on different model parameters without the requirement of intensive Monte Carlo simulations.

D. Model parameter dependence

Given the validity domain of Corollary 1 as established in Sec. III B, one can now use the explicit expression for the conditional variance of τ_+ in Corollary 1 to study how the uncertainties of RI onset time vary with different model parameters and/or initial conditions. This knowledge is important for practical applications, because it helps forecasters estimate the uncertainties of their RI onset prediction for different environmental conditions or ocean basins in real-time forecast.

We recall that the dependence of (22) on different parameters is most useful if an estimation of the deterministic RI onset time T, say from a numerical or a statistical model, is given. As a result, Fig. 8 shows the deterministic onset time T for different initial condition v_0 and model parameters (p, r, s). Here, the same hitting level $\ell = 0.1$ at which the RI onset is considered to occur is used.

As shown in Fig. 8(a), T is inversely proportional to v_0 as expected, which implies that RI onset will occur earlier for stronger initial intensity. When fixing TC initial condition, we note, however, that T increases roughly linearly when the model parameter s or r increases. This linear relationship indicates that a more stable troposphere or stronger radiative cooling will delay RI onset as seen in Figs. 8(b) and 8(c). In contrast, RI onset tends to occur earlier for larger parameter p [Fig. 8(d)], suggesting that a bigger storm size would require less time for RI to take place. These behaviors can be used to validate our results, using observational data or modeling output that we will present in our future study.

Given the deterministic RI onset time T, one can now look into how the uncertainty of RI onset time changes with different model parameters. Among all the model parameters, it is of interest to note that the conditional variance of τ_+, which is summarized by the function $H(T) \equiv \frac{\Sigma_{22}(T)}{\ell^2\,[u(T)+\ell]^2}$, appears to be the least sensitive to changes in the model parameter p (Fig. 9). On the other hand, the variance of τ_+

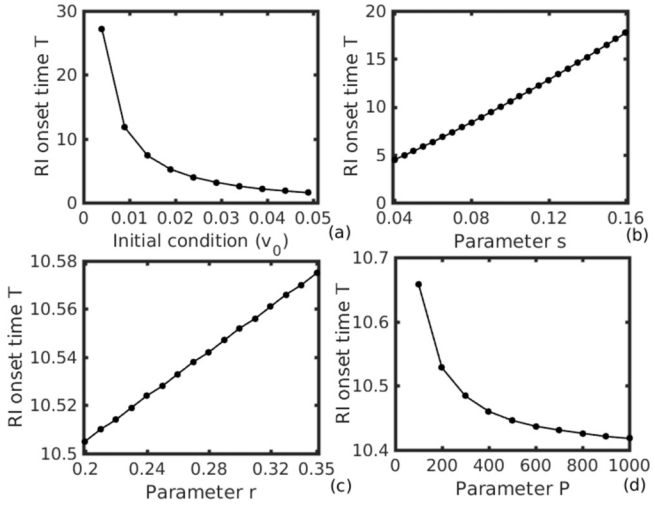

FIG. 8. Dependence of the deterministic RI onset time T on (a) the initial condition v_0, (b) the atmospheric static stability parameter s, (c) the radiative cooling parameter r, and (d) the aspect ratio of the tropospheric depth over the radius of maximum wind p. We note that for each parameter curve, all other parameters are fixed at the values of $p = 200$, $s = 0.1$, $r = 0.25$, $u_0 = -0.01$, $v_0 = 0.01$, $b_0 = 0.0001$.

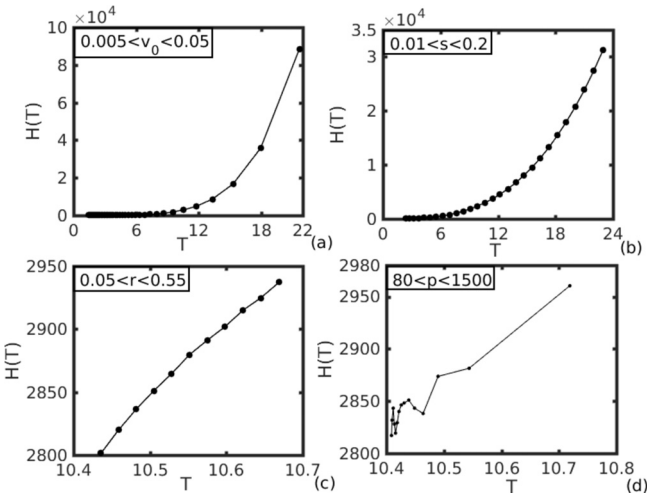

FIG. 9. Similar to Fig. 8 but for the function $H(T)$ in the variance formula of Corollary 1.

tends to be sensitive to both the radiative cooling (r) and the tropospheric stratification (s) parameter [Figs. 9(c) and 9(d)]. This sensitivity of $H(T)$ to these specific model parameters r and s reveals how the large-scale environmental factors can affect RI onset variability, for which TC models must take into account to properly capture RI onset variability in the future implementation.

V. CONCLUSION

In this paper, the rapid intensification (RI) process of tropical cyclone (TC) development was examined, using the first hitting time and asymptotic analysis for stochastic systems. By extending the TC-scale dynamical model (MSD) for TC development proposed by Kieu,[23] RI can be considered as a random process whose onset time possesses a specific probability distribution dictated by TC dynamics. The reduced dynamics of the MSD model in the phase space of TC scales (u, v, b) makes it especially attractive for studying RI, because one can obtain analytical results that could not be obtained otherwise with full-physics models.

Specifically, by defining RI onset time as the first moment that TC intensity hits a given level ℓ, a formal procedure to derive the RI onset probability $p(\mathbf{x})$ was obtained in Lemma III.1 through a boundary value problem. While the explicit expression for $p(\mathbf{x})$ has to be relied on numerical integration, its asymptotic limit $\varepsilon \to 0$ could indicate that the probability of RI onset will be ensured for all initial conditions with $v_0 > 0$, consistent with previous modeling studies of TC development.

Conditioned on the RI onset occurrence, we showed that the timing of RI onset (τ_+) would be on average longer for weaker vortex initial condition v_0. Also, RI onset timing will have larger uncertainty when the random noise amplitude ε increases, with an asymptotic variance expression given by Corollary 1 in the small noise limit. In this small noise regime, we also demonstrated that larger random noise ε tends to cause smaller probability for RI onset and a smaller conditional expectation for RI onset time. The latter observation is important, because it helps alert forecasters a possible earlier RI onset in the presence of larger random fluctuation.

Our main mathematical result regarding the variability of the RI onset time τ_+ is provided by Corollary 1, which presents an asymptotic formula for the conditional variance of τ_+ in the small noise regime. Detailed examination of this variance formula using an efficient algorithm to numerically compute it from any given initial state showed that the variability of RI onset timing depends critically on TC initial intensity as well as model parameters. For a fixed set of model parameters, the variance of RI onset time decreases with initial intensity v_0. That is, *an initially stronger vortex would experience not only earlier RI onset time but also less uncertainty in the prediction of the timing of RI onset*. Similarly, the uncertainties in RI onset time will be smaller when the model parameters such as atmospheric stability (s) or the aspect ratio (p) decreases, suggesting a strong dependence of the RI onset forecast on the atmospheric large-scale condition.

To determine the domain of validity of our theoretical results, Monte Carlo simulations of the MSD system were also conducted, using the same set of parameters and initial conditions as those obtained from the theoretical analyses. Our examination of these Monte Carlo simulations for different asymptotic limits of random noise amplitude ε confirmed the validity of the theoretical results for the limit of $\varepsilon \to 0$. These simulations helped verify several hypotheses that were assumed in our lemmas and theorems, thus providing a range of limits that our theoretical results can be applied in real TC systems.

From the mathematical perspective, we note an intriguing fact that several results on the RI onset probability and timing derived from the MSD system can be understood by using a one-dimensional (1D) stochastic system. Our analyses of a general 1D stochastic equation could indeed capture well key properties of the probability distribution of RI onset as well as the timing of RI onset as in the MSD system. In this regard, these analyses suggest that the method and results in this study can be applied to more generic stochastic systems that possess the first hitting time characteristic, so long as the evolution of the systems prior to a rapid change in the system can be considered as a slow process. Further exploration of the first hitting time for such general 1D stochastic systems will be presented in our future work.

ACKNOWLEDGMENTS

This research was partially supported by the ONR/DRI Award No. N000142012411 and the NSF Award No. DMS-1804492. D.S. wish to also thank "Andreas Mentzelopoulos Scholarships University of Patras" for their financial support during his doctoral program at Indiana University. We thank three anonymous reviewers for their constructive comments and suggestions.

APPENDIX: PROOFS FOR GENERAL 1-DIMENSIONAL DIFFUSIONS

In this section, we provide the proofs of our results in Sec. III C. The following asymptotic properties for the error function will be useful in several places in our proofs: for all $c \in (0, \infty)$, as $\varepsilon \to 0$, we have

$$erf(c\,\varepsilon^{\alpha-1}) \sim \begin{cases} 1 & \text{if } \alpha \in (0,1), \\ erf(c) & \text{if } \alpha = 1, \\ \dfrac{2c}{\sqrt{\pi}}\varepsilon^{\alpha-1} & \text{if } \alpha \in (1,\infty). \end{cases} \tag{A1}$$

Here, $A \sim B$ means $\lim_{\varepsilon\to 0} A/B = 1$.

Proof 4 (Proof of Lemma III.4). *Let* $h(x) = \mathbb{P}_x(\tau_\ell < \tau_0)$. *Then as in the proof of Lemma III.1, the function h satisfies the following boundary value problem:*

$$\frac{\varepsilon^2}{2}h''(x) + F(x)h'(x) = 0 \quad \text{if} \quad 0 < x < \ell,$$
$$h(\ell) = 1 \quad \text{and} \quad h(0) = 0.$$

Upon solving this equation for h using the integrating factor k_ε *given by (32), we obtain the desired formula.* □

Proof 5 (Proof of Theorem III.5). *This result and the proof are similar to that of Ref. 41* (Lemma 6), *which is a variation of the Laplace method. For all* $t \in (0,\infty)$, *there exists* $\xi_t \in (0,t)$ *such that*

$$F(t) = F'(0)t + \frac{F''(\xi_t)}{2}t^2. \tag{A2}$$

To simplify notation, we introduce

$$f_1(y) := \int_0^y F(t)\,dt, \tag{A3}$$
$$f_2(y) := \int_0^y F'(0)t\,dt = F'(0)\frac{y^2}{2},$$
$$I(x) := \int_0^x \exp\left(\frac{-2}{\varepsilon^2}f_1(y)\right)dy,$$
$$\tilde{I}(x) := \int_0^x \exp\left(\frac{-2}{\varepsilon^2}f_2(y)\right)dy. \tag{A4}$$

By Lemma III.4

$$\mathbb{P}_{c\varepsilon^\alpha}(\tau_\ell < \tau_0) = \frac{I(c\,\varepsilon^\alpha)}{I(\ell)}. \tag{A5}$$

For all $y>0$, *we have* $|f_1(y) - f_2(y)| = |\int_0^y F(t)\,dt - \int_0^y F'(0)t\,dt| \le \frac{|F''(\xi_t)|}{6}y^3$. *Hence for* $y < c\varepsilon^\alpha$

$$|f_1(y) - f_2(y)| \le \frac{|F''(\xi_t)|}{6}c^3\varepsilon^{3\alpha}. \tag{A6}$$

Since F is smooth, $M := \sup_{y\in[0,c\varepsilon^\alpha]}|F''(y)| < \infty$. *Therefore,*

$$\begin{aligned}|I(c\,\varepsilon^\alpha) - \tilde{I}(c\,\varepsilon^\alpha)| &= \left|\int_0^{c\varepsilon^\alpha}\exp\left(\frac{-2}{\varepsilon^2}f_1(y)\right) - \exp\left(\frac{-2}{\varepsilon^2}f_2(y)\right)dy\right| \\ &= \left|\int_0^{c\varepsilon^\alpha}\int_{[f_1(y),f_2(y)]}\frac{-2}{\varepsilon^2}e^{\frac{-2}{\varepsilon^2}x}\,dx\,dy\right| \\ &\le \frac{2}{\varepsilon^2}\int_0^{c\varepsilon^\alpha}\sup_{[f_1(y),f_2(y)]}e^{\frac{-2}{\varepsilon^2}x}\cdot|f_1(y) - f_2(y)|\,dy \\ &\le \frac{c^4}{3}M\varepsilon^{2(2\alpha-1)},\end{aligned}$$

where in the last step we used (A6). From this, we have

$$\left|\frac{I(c\,\varepsilon^\alpha) - \tilde{I}(c\,\varepsilon^\alpha)}{I(\ell)}\right| \le \frac{c^4}{3}\,M\,\frac{\varepsilon^{4\alpha-3}}{\varepsilon^{-1}I(\ell)}. \tag{A7}$$

For the integral $I(\ell)$ *in the denominator, we note that* $g(y) := -2f_1(y)$ *is decreasing in* $[0,\ell]$, *and thus, it has maximum at* $c=0$ *the* $g(0) = 0$. *We also note that* $g'(0) = -2F(0) = 0$. *By Laplace method, as* $\varepsilon \to 0$

$$I(\ell) = \int_0^\ell \exp\left(\frac{-2}{\varepsilon^2}f_1(y)\right)dy \sim \sqrt{\frac{\pi}{F'(0)}}\frac{\varepsilon}{2}. \tag{A8}$$

From this and (A7), we see that for $\alpha > \frac{3}{4}$

$$\lim_{\varepsilon\to 0}\frac{I(c\,\varepsilon^\alpha)}{I(\ell)} = \lim_{\varepsilon\to 0}\frac{\tilde{I}(c\,\varepsilon^\alpha)}{I(\ell)}. \tag{A9}$$

By the change of variable $u = \sqrt{F'(0)}\frac{y}{\varepsilon}$

$$\begin{aligned}\tilde{I}(c\,\varepsilon^\alpha) &= \int_0^{c\varepsilon^\alpha}\exp\left(\frac{-F'(0)}{\varepsilon^2}y^2\right)dy \\ &= \frac{\varepsilon}{\sqrt{F'(0)}}\int_0^{c\sqrt{F'(0)}\varepsilon^{\alpha-1}} e^{-u^2}\,du \\ &= \frac{\varepsilon}{2}\sqrt{\frac{\pi}{F'(0)}}erf(c\sqrt{F'(0)}\varepsilon^{\alpha-1}).\end{aligned}$$

So for $\alpha > \frac{3}{4}$, *as* $\varepsilon \to 0$, *by (A9) we have*

$$\frac{I(c\,\varepsilon^\alpha)}{I(\ell)} \sim \frac{\tilde{I}(c\,\varepsilon^\alpha)}{I(\ell)} = \frac{\frac{\varepsilon}{2}\sqrt{\frac{\pi}{F'(0)}}}{I(\ell)}erf(c\sqrt{F'(0)}\varepsilon^{\alpha-1}) \sim erf(c\sqrt{F'(0)}\varepsilon^{\alpha-1}), \tag{A10}$$

where in the last step, we used (A8). From (A1), (A5), and (A10), we obtain the desired equality for $\alpha > 3/4$.

The remaining case $\alpha \in (0, 3/4]$ *is covered, because* $\mathbb{P}_x(\tau_\ell < \tau_0)$ *is monotonically increasing in x and* $\varepsilon^{\alpha_1} < \varepsilon^{\alpha_2}$ *if* $\alpha_1 > \alpha_2 > 0$. *The proof is complete.* □

Proof 6 (Proof of Lemma III.6). *Let* $\tau = \min\{\tau_\ell, \tau_0\} = \inf\{t \ge 0 : Z_t = 0 \text{ or } \ell\}$ *be the time to exit the interval* $(0,\ell)$. *We shall show that for any starting point* $x \in [0,\ell]$

$$\mathbb{E}_x[\tau 1_{\{\tau_\ell<\tau_0\}}] = \frac{2}{\varepsilon^2}\frac{1}{\int_0^\ell k_\varepsilon(z)dz}\left\{\int_x^\ell\int_0^x k_\varepsilon(z)k_\varepsilon(u)\int_u^z\frac{p(y)}{k_\varepsilon(y)}\,dy\,du\,dz\right\}. \tag{A11}$$

We recall that $p(x) = \mathbb{P}_x(\tau_\ell < \tau_0)$ *and that by Lemma III.4,* $p(x) = \frac{\int_0^x k_\varepsilon(y)\,dy}{\int_0^\ell k_\varepsilon(y)\,dy}$. *The function H defined by* $H(x) = \mathbb{E}_x[\tau\,1_{\{\tau_\ell<\tau_0\}}]$ *solves the boundary value problem*

$$p(x) + \frac{\varepsilon^2}{2}H''(x) + F(x)\,H'(x) = 0 \quad \text{if} \quad 0 < x < \ell, \tag{A12}$$
$$H(0) = H(\ell) = 0. \tag{A13}$$

We now solve (A12) and (A13) to obtain (A11). Note that (A12) is a first-order equation in $H'(x)$, *given by*

$$H''(x) + \frac{2}{\varepsilon^2}F(x)H'(x) = \frac{-2}{\varepsilon^2}p(x). \tag{A14}$$

We multiply both sides by the integrating factor $k_\varepsilon^{-1}(x) = \exp\{\int_0^x \frac{2}{\varepsilon^2}F(t)\,dt\}$

$$\left[H'(x)k_\varepsilon^{-1}(x)\right]' = \frac{-2}{\varepsilon^2}k_\varepsilon^{-1}(x)p(x),$$
$$H'(x) = \frac{-2}{\varepsilon^2}k_\varepsilon(x)K(x) + Ck_\varepsilon(x),$$

where we let $K(x) = \int_0^x k_\varepsilon^{-1}(y)p(y)\,dy$ *for simplicity.*

Integrating again and using the fact $H(0) = 0$*, we have*

$$H(x) - 0 = -\frac{2}{\varepsilon^2}\int_0^x k_\varepsilon(z)\,K(z)\,dz + C\int_0^x k_\varepsilon(z)\,dz.$$

To compute C, we use the fact that $H(\ell) = 0$*. We find that*

$$C = \frac{\frac{2}{\varepsilon^2}\int_0^\ell k_\varepsilon(z)\,K(z)\,dz}{\int_0^\ell k_\varepsilon(z)dz}.$$

From the last two displayed equations

$$\begin{aligned}H(x) &= -\frac{2}{\varepsilon^2}\int_0^x k_\varepsilon(z)\,K(z)\,dz + \frac{\frac{2}{\varepsilon^2}\int_0^\ell k_\varepsilon(z)\,K(z)\,dz}{\int_0^\ell k_\varepsilon(z)dz}\cdot\int_0^x k_\varepsilon(z)\,dz\\ &= \frac{2}{\varepsilon^2}\left\{\int_0^\ell k_\varepsilon(z)\,K(z)\,dz\cdot\frac{\int_0^x k_\varepsilon(z)\,dz}{\int_0^\ell k_\varepsilon(z)dz} - \int_0^x k_\varepsilon(z)\,K(z)\,dz\right\}\\ &= \frac{2}{\varepsilon^2}\left\{\int_0^\ell k_\varepsilon(z)\,K(z)\,dz\cdot p(x) - \int_0^x k_\varepsilon(z)\,K(z)\,dz\right\}. \qquad \text{(A15)}\end{aligned}$$

We now rewrite (A15) in a way that reflects why the complicated expression on the right is non-negative

$$\begin{aligned}H(x) &= \frac{2}{\varepsilon^2}\left\{\int_0^\ell k_\varepsilon(z)\,K(z)\,dz\cdot\frac{\int_0^x k_\varepsilon(z)\,dz}{\int_0^\ell k_\varepsilon(z)dz} - \int_0^x k_\varepsilon(z)\,K(z)\,dz\right\}\\ &= \frac{2}{\varepsilon^2}\frac{1}{\int_0^\ell k_\varepsilon(z)dz}\left\{\int_0^\ell k_\varepsilon(z)K(z)\,dz\int_0^x k_\varepsilon(z)\,dz\right.\\ &\quad\left. - \int_0^\ell k_\varepsilon(z)dz\int_0^x k_\varepsilon(z)K(z)\,dz\right\}\\ &= \frac{2}{\varepsilon^2}\frac{1}{\int_0^\ell k_\varepsilon(z)dz}\left\{\int_x^\ell\int_0^x k_\varepsilon(z)k_\varepsilon(u)(K(z)-K(u))\,du\,dz\right\},\end{aligned}$$

where in the last equality, we have used the fact (by symmetry) that $\int_0^x\int_0^x k_\varepsilon(z)k_\varepsilon(u)(K(z)-K(u))\,du\,dz = 0$*. In conclusion, we proved (A11). The lemma then follows from (A11).* □

Proof 7 (Proof of Theorem III.7). *We recall the formula (34) in Lemma III.6. Fix* $\varepsilon > 0$ *and let* $x \to 0$*, the denominator in (34) is of order x in the sense that*

$$\lim_{x\to 0}\frac{\int_0^x k_\varepsilon(z)dz}{x} = k_\varepsilon(0) = 1. \qquad \text{(A16)}$$

The numerator of (34) is also of order x in the sense that

$$\lim_{x\to 0}\frac{1}{x}\int_x^\ell\int_0^x k_\varepsilon(z)k_\varepsilon(u)\int_u^z\frac{p(y)}{k_\varepsilon(y)}\,dy\,du\,dz = \int_0^\ell k_\varepsilon(u)\int_0^u\frac{p(y)}{k_\varepsilon(y)}\,dy\,du. \qquad \text{(A17)}$$

Equation (A17) follows from the L'Hospital rule and the Leibniz integral rule as follows. We define

$$\begin{aligned}L(x) &:= \int_x^\ell\int_0^x k_\varepsilon(z)k_\varepsilon(u)\int_u^z\frac{p(y)}{k_\varepsilon(y)}\,dy\,du\,dz,\\ F_1(x,z) &:= \int_0^x k_\varepsilon(z)k_\varepsilon(u)\int_u^z\frac{p(y)}{k_\varepsilon(y)}\,dy\,du,\\ G_1(z,u) &:= k_\varepsilon(z)k_\varepsilon(u)\int_u^z\frac{p(y)}{k_\varepsilon(y)}\,dy.\end{aligned}$$

Then, $L(x) = \int_x^\ell F_1(x,z)\,dz$ *and* $F_1(x,z) = \int_0^x G_1(z,u)\,du$*. By Leibniz integral rule*

$$\begin{aligned}L'(x) &= -F_1(x,x) + \int_x^\ell\frac{\partial}{\partial x}F_1(x,z)\,dz\\ &= -k_\varepsilon(x)\int_0^x k_\varepsilon(u)\int_u^x\frac{p(y)}{k_\varepsilon(y)}\,dy\,du + \int_x^\ell G_1(z,x)\,dz\\ &= k_\varepsilon(x)\int_0^x k_\varepsilon(u)\int_x^u\frac{p(y)}{k_\varepsilon(y)}\,dy\,du + k_\varepsilon(x)\int_x^\ell k_\varepsilon(u)\int_x^u\frac{p(y)}{k_\varepsilon(y)}\,dy\,du\\ &= k_\varepsilon(x)\left\{\int_0^\ell k_\varepsilon(u)\int_x^u\frac{p(y)}{k_\varepsilon(y)}\,dy\,du\right\}.\end{aligned}$$

Letting $x \to 0$ *and applying L'Hospital rule, we obtain (A17). By (A16) and (A17), the proof of (36) is complete. The second and the third derivatives of L(x) are*

$$\begin{aligned}L''(x) &= k_\varepsilon'(x)\int_0^\ell k_\varepsilon(u)\int_x^u\frac{p(y)}{k_\varepsilon(y)}\,dy\,du - p(x)\int_0^\ell k_\varepsilon(u)\,du,\\ L^{(3)}(x) &= k_\varepsilon'(x)\int_0^\ell k_\varepsilon(u)\int_x^u\frac{p(y)}{k_\varepsilon(y)}dydu - \frac{k_\varepsilon'(x)p(x)}{k_\varepsilon(x)}\int_0^\ell k_\varepsilon(u)du\\ &\quad -p'(x)\int_0^\ell k_\varepsilon(u)du.\end{aligned}$$

We note that $k_\varepsilon'(x) = \frac{-2}{\varepsilon^2}F(x)\,k_\varepsilon(x)$*, so* $F(0) = 0$ *implies* $k_\varepsilon'(0) = 0$*. Furthermore,* $k_\varepsilon''(0) = \frac{-2}{\varepsilon^2}F'(0) < 0$ *since* $F'(0) > 0$*. These give* $L''(0) = 0$ *and*

$$L^{(3)}(0) = \frac{-2F'(0)}{\varepsilon^2}\,C - 1 < 0,$$
$$\text{where } C = \int_0^\ell k_\varepsilon(u)\int_0^u\frac{p(y)}{k_\varepsilon(y)}\,dy\,du = L'(0).$$

We note that

$$\mathbb{E}_x[\tau_\ell\,|\,\tau_\ell < \tau_0] - \Psi(\varepsilon) = \frac{2}{\varepsilon^2}\left(\frac{L(x)}{\int_0^x k_\varepsilon(z)dz} - L'(0)\right).$$

Hence,

$$
\begin{aligned}
&\lim_{x\to 0}\frac{\mathbb{E}_x[\tau_\ell \mid \tau_\ell < \tau_0] - \Psi(\varepsilon)}{x^2}\\
&= \frac{2}{\varepsilon^2}\lim_{x\to 0}\frac{L(x) - L'(0)\int_0^x k_\varepsilon(z)dz}{x^2\int_0^x k_\varepsilon(z)dz}\\
&= \frac{2}{\varepsilon^2}\lim_{x\to 0}\frac{L'(x) - L'(0)\,k_\varepsilon(x)}{x^2k_\varepsilon(x) + 2x\displaystyle\int_0^x k_\varepsilon(z)dz}\\
&= \frac{2}{\varepsilon^2}\lim_{x\to 0}\frac{L''(x) - L'(0)\,k'_\varepsilon(x)}{x^2k'_\varepsilon(x) + 4xk_\varepsilon(x) + 2\displaystyle\int_0^x k_\varepsilon(z)dz}\\
&= \frac{2}{\varepsilon^2}\lim_{x\to 0}\frac{L^{(3)}(x) - L'(0)\,k''_\varepsilon(x)}{x^2k''_\varepsilon(x) + 6xk'_\varepsilon(x) + 6k_\varepsilon(x)}\\
&= \frac{2}{\varepsilon^2}\frac{L^{(3)}(0) - L'(0)\,k''_\varepsilon(0)}{6}\\
&= \frac{1}{3\varepsilon^2}\left(\frac{-2F'(0)}{\varepsilon^2}\,C - 1\right) + C\,\frac{2F'(0)}{\varepsilon^2}\\
&= \frac{-1}{3\varepsilon^2}.
\end{aligned}
$$

□

DATA AVAILABILITY

The data that support the findings of this study are available within the article.

REFERENCES

[1]Practically, RI is defined as a change of the maximum 10 m wind of 30 kt (15 ms^{-1} in 24 h).

[2]J. Kaplan and M. DeMaria, "Large-scale characteristics of rapidly intensifying tropical cyclones in the North Atlantic basin," Weather Forecast. **18**, 1093–1108 (2003).

[3]C. R. Sampson, J. Kaplan, J. A. Knaff, M. DeMaria, and C. A. Sisko, "A deterministic rapid intensification aid," Weather Forecast. **26**, 579–585 (2011).

[4]E. N. Rappaport, J.-G. Jiing, C. W. Landsea, S. T. Murillo, and J. L. Franklin, "The joint hurricane test bed: Its first decade of tropical cyclone research-to-operations activities reviewed," Bull. Am. Meteorol. Soc. **93**, 371–380 (2012).

[5]M. S. Fischer, B. H. Tang, and K. L. Corbosiero, "A climatological analysis of tropical cyclone rapid intensification in environments of upper-tropospheric troughs," Mon. Weather Rev. **147**, 3693–3719 (2019).

[6]R. Kowch and K. Emanuel, "Are special processes at work in the rapid intensification of tropical cyclones?," Mon. Weather Rev. **143**, 878–882 (2015).

[7]P. Nguyen, C. Kieu, and W.-T. L. Fan, "Stochastic variability of tropical cyclone intensity at the maximum potential intensity equilibrium," J. Atmos. Sci. **77**, 3105–3118 (2020).

[8]J. Kaplan, C. M. Rozoff, M. DeMaria, C. R. Sampson, J. P. Kossin, C. S. Velden, J. J. Cione, J. P. Dunion, J. A. Knaff, J. A. Zhang, J. F. Dostalek, J. D. Hawkins, T. F. Lee, and J. E. Solbrig, "Evaluating environmental impacts on tropical cyclone rapid intensification predictability utilizing statistical models," Weather Forecast. **30**, 1374–1396 (2015).

[9]V. Tallapragada, C. Kieu, S. Trahan, Q. Liu, W. Wang, Z. Zhang, M. Tong, B. Zhang, L. Zhu, and B. Strahl, "Forecasting tropical cyclones in the Western North Pacific basin using the NCEP operational HWRF model: Model upgrades and evaluation of real-time performance in 2013," Weather Forecast. **31**, 877–894 (2016).

[10]V. Tallapragada, C. Kieu, Y. Kwon, S. Trahan, Q. Liu, Z. Zhang, and I.-H. Kwon, "Evaluation of storm structure from the operational HWRF during 2012 implementation," Mon. Weather Rev. **142**, 4308–4325 (2014).

[11]C. M. Rozoff, C. S. Velden, J. Kaplan, J. P. Kossin, and A. J. Wimmers, "Improvements in the probabilistic prediction of tropical cyclone rapid intensification with passive microwave observations," Weather Forecast. **30**, 1016–1038 (2015).

[12]R. Yang, "A systematic classification investigation of rapid intensification of Atlantic tropical cyclones with the SHIPS database," Weather Forecast. **31**, 495–513 (2016).

[13]A. J. Majda, I. Timofeyev, and E. V. Eijnden, "Models for stochastic climate prediction," Proc. Natl. Acad. Sci. U. S. A. **96**, 14687–14691 (1999).

[14]C. Q. Kieu and Z. Moon, "Hurricane intensity predictability," Bull. Am. Meteorol. Soc. **97**, 1847–1857 (2016).

[15]D. James, D. S. Chen, Y. Jin, J. R. Moskaitis, S. Wang, E. A. Hendricks, H. Jin, and T. A. Smith, "Tropical cyclone prediction using COAMPS-TC," Oceanography **27**, 104–115 (2015).

[16]H. Jin, M. S. Peng, Y. Jin, and J. D. Doyle, "An evaluation of the impact of horizontal resolution on tropical cyclone predictions using COAMPS-TC," Weather Forecast. **29**, 252–270 (2014).

[17]C. Kieu, C. Evans, Y. Jin, J. D. Doyle, H. Jin, and J. Moskaitis, "Track dependence of tropical cyclone intensity forecast errors in the COAMPS-TC model," Weather Forecast. **36**, 469–485 (2021).

[18]E. L. Navarro and G. J. Hakim, "Idealized numerical modeling of the diurnal cycle of tropical cyclones," J. Atmos. Sci. **73**, 4189–4201 (2016).

[19]S. Rasp, T. Selz, and G. C. Craig, "Variability and clustering of midlatitude summertime convection: Testing the Craig and Cohen theory in a convection-permitting ensemble with stochastic boundary layer perturbations," J. Atmos. Sci. **75**, 691–706 (2018).

[20]G. H. Bryan, N. A. Dahl, D. S. Nolan, and R. Rotunno, "An eddy injection method for large-eddy simulations of tornado-like vortices," Mon. Weather Rev. **145**, 1937–1961 (2017).

[21]C. Kieu, K. Keshavamurthy, V. Tallapragada, S. Gopalakrishnan, and S. Trahan, "On the growth of intensity forecast errors in the operational hurricane weather research and forecasting (HWRF) model," Q. J. R. Meteorol. Soc. **144**, 1803–1819 (2018).

[22]C. Q. Kieu and Q. Wang, "Stability of tropical cyclone equilibrium," J. Atmos. Sci. **74**, 3591–3608 (2017).

[23]C. Q. Kieu, "Hurricane maximum potential intensity equilibrium," Q. J. R. Meteorol. Soc. **141**, 2471–2480 (2015).

[24]A. Budhiraja and W.-T. L. Fan, "Uniform in time interacting particle approximations for nonlinear equations of Patlak–Keller–Segel type," Electron. J. Probab. **22**, 1–37 (2017).

[25]I. Karatzas and S. E. Shreve, *Brownian Motion and Stochastic Calculus*, 2nd ed., Graduate Texts in Mathematics Vol. 113 (Springer-Verlag, NY, 1991), pp. xxiv+470.

[26]S. N. Ethier and T. G. Kurtz, *Markov Processes: Characterization and Convergence*, Wiley Series in Probability and Mathematical Statistics: Probability and Mathematical Statistics (John Wiley & Sons, Inc., NY, 1986), pp. x+534.

[27]S. A. A. Monter and Y. Bakhtin, "Scaling limit for the diffusion exit problem in the Levinson case," arXiv:1006.2766 (2010).

[28]R. F. Bass, *Probabilistic Techniques in Analysis* (Springer Science & Business Media, 1994).

[29]Y. Bakhtin and Z. Pajor-Gyulai, "Scaling limit for escapes from unstable equilibria in the vanishing noise limit: Nontrivial Jordan block case," arXiv:1708.00558 (2017).

[30]P. Kloeden and E. Platen, *Numerical Solution of Stochastic Differential Equations* (Springer, Berlin, 1992), p. 518.

[31]M. S. Fischer, B. H. Tang, K. L. Corbosiero, and C. M. Rozoff, "Normalized convective characteristics of tropical cyclone rapid intensification events in the North Atlantic and Eastern North Pacific," Mon. Weather Rev. **146**, 1133–1155 (2018).

[32]C. Q. Kieu, V. Tallapragada, and W. A. Hogsett, "On the onset of the tropical cyclone rapid intensification in the HWRF model," Geophys. Res. Lett. **41**, 3298–3306, https://doi.org/10.1002/2014GL059584 (2014).

[33]W. Shen, R. E. Tuleya, and I. Ginis, "A sensitivity study of the thermodynamic environment on GDFL model hurricane intensity: Implications for global warming," J. Clim. **13**, 109–121 (2000).

[34]K. A. Hill and G. M. Lackmann, "The impact of future climate change on TC intensity and structure: A downscaling approach," J. Clim. **24**, 4644–4661 (2011).
[35]R. E. Tuleya, M. Bender, T. R. Knutson, J. J. Sirutis, B. Thomas, and I. Ginis, "Impact of upper-tropospheric temperature anomalies and vertical wind shear on tropical cyclone evolution using an idealized version of the operational GDFL hurricane model," J. Atmos. Sci. **73**, 3803–3820 (2016).
[36]Z. Moon and C. Kieu, "Impacts of the lower stratosphere on the development of intense tropical cyclones," Atmosphere **8**, 128 (2017).
[37]M. Ferrara, F. Groff, Z. Moon, K. Keshavamurthy, S. M. Robeson, and C. Kieu, "Large-scale control of the lower stratosphere on variability of tropical cyclone intensity," Geophys. Res. Lett. **44**, 4313, https://doi.org/10.1002/2017GL073327 (2017).
[38]C. Kieu and D.-L. Zhang, "The control of environmental stratification on the hurricane maximum potential intensity," Geophys. Res. Lett. **45**, 6272–6280, https://doi.org/10.1029/2018GL078070 (2018).
[39]A. Downs and C. Kieu, "A look at the relationship between the large-scale tropospheric static stability and the tropical cyclone maximum intensity," J. Clim. **33**, 959–975 (2020).
[40]C. Tao and H. Jiang, "Distributions of shallow to very deep precipitation–convection in rapidly intensifying tropical cyclones," J. Clim. **28**, 8791–8824 (2015).
[41]B. McLoone, W.-T. L. Fan, A. Pham, R. Smead, and L. Loewe, "Stochasticity, selection, and the evolution of cooperation in a two-level Moran model of the snowdrift game," Complexity **2018**, 9836150.